School of Chemistry

Optimisation of growth conditions of diamond films in a microwave plasma CVD reactor, for potential use as tritium detectors.

Hannah Richards

April 2022

This thesis is submitted in partial fulfilment of the requirements for the Honours Degree of MSci at the University of Bristol

Supervisor - Neil Fox
Second Assessor - Paul May
Section - Physical and Theoretical

Abstract

Diamond has lots of unique and valuable properties that make it a desirable material for many applications, one of which is radiation detection. When radiation interacts with a diamond crystal it causes the formation of electrons and positive ions (holes), which, when a potential difference is applied, can be detected as a current. Tritium decays *via* beta decay and the aim of this project was to fabricate a device that could detect the beta particles produced during the decay of tritium.

Single crystal diamond (SCD) is the ideal substrate for use as a diamond detector due to its lack of grain boundaries, which prevent the electrons and holes being detected. The established method of growing SCD, using chemical vapour deposition (CVD), initially involves a technique called biased enhanced nucleation and uses iridium as a substrate. Biased enhanced nucleation was not possible with the facilities available, therefore it was decided that in order to grow diamond for potential use in tritium detectors, the conditions used for microwave plasma CVD would be optimised to grow the largest, most uniform grains of polycrystalline diamond. The conditions were optimised using silicon substrates, grown at varying pressures and methane concentrations whilst keeping constant the power (1200 W) and total flow rate (600 standard cubic centimetres per minute (sccm)). Scanning electron microscopy (SEM) images were used to analyse the films and the results showed that the sample run at 120 torr and 10% methane produced the best grains, with an average grain size of about 6 μm. These conditions were then used to grow diamond on iridium substrates, given iridium's success at enabling SCD growth. However, this resulted in very low-quality, "ballas" diamond, so was not used any further.

A first set of potential device designs were fabricated using polycrystalline diamond grown on molybdenum, as a conducting surface was required on the bottom of the diamond film. The grains were not as uniform or as large as those grown on silicon but showed huge improvement over the iridium samples. SCD substrates were also acquired and used to fabricate a set of devices for comparison. Initial current leakage measurements indicated that the single crystal detectors showed suitably small leakage currents, however the polycrystalline devices gave leakage currents six orders of magnitude larger, and these initial devices were therefore expected to be unsuitable as radiation detectors. Both sets of devices will undergo radiation testing in order to further assess their effectiveness as detectors.

Overall, it was shown that not only the conditions, but also the substrates can significantly influence the quality, size and growth rate of the grains. The silicon substrates, used in the optimisation process, gave the best films and the iridium substrates gave very poor quality diamond. Several different device designs were fabricated and initial results concluded, as expected, that the SCD devices would be the most effective as tritium detectors.

Acknowledgements

I would like to thank my supervisor, Professor Neil Fox for all his help and for making this project possible. Thanks to Ed Smith for his help in the diamond lab and many hours doing SEM, I could not have done it without him. Thanks to Professor Paul May for the advice he has given me and the diamond group as a whole for being so welcoming and always willing to help.

Contents

1 Introduction

1.1 Diamond as a material

1.1.1 Properties and structure of diamond

Diamond is the world's hardest material (mechanical hardness $\sim$ 90 GPa) and is highly prized both by the scientific community and the public. Its useful properties include chemical inertness, high thermal conductivity (2 x 10^3 $Wm^{-1}K^{-1}$) and low thermal expansion (0.8 x 10^{-6} K^{-1}) along with many others. Despite being less stable than graphite at ambient pressure and temperature, diamond is the densest form of carbon and therefore is the most stable form at high pressures.[1]

Diamond consists of a crystal lattice of tetrahedral sp^3 carbon atoms with a bond length of 1.54 Å (figure 1a). The structure is a face-centred cubic (FCC) arrangement within the unit cell (figure 1b). This rigid covalent structure gives rise to the unique properties of diamond. The other common allotrope of carbon, graphite, has shorter bonds of 1.42 Å, caused by the sp^2 nature of the carbon atoms which are arranged in planar hexagonal layers (figure 1c). Three sp^2 hybridised orbitals overlap to form three σ bonds between adjacent carbons and the remaining p orbitals overlap to form a delocalised π bonding network. This explains why graphite is a much softer material than diamond and the delocalised system of electrons accounts for the conductivity of graphite.[2] Figure 1 shows the differences between the structures of the two carbon allotropes.

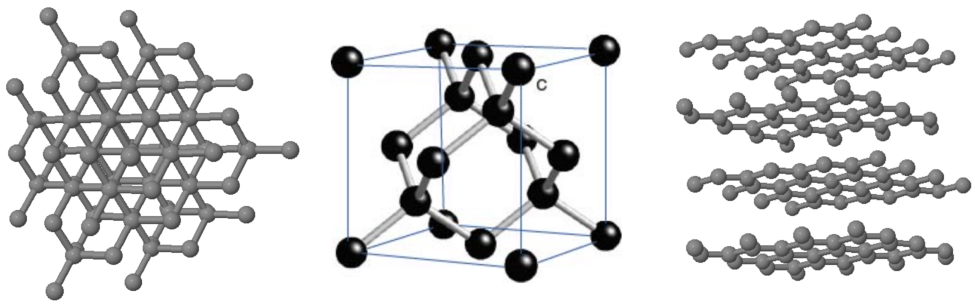

(a) (b) (c)

Figure 1: *Structures of a) diamond lattice, b) diamond unit cell showing FCC structure and c) graphite showing the layers formed.*[3]

Depending on the conditions, the growth of diamond can be orientated along different crystallographic surfaces resulting in different surface structures for the diamond. The two most common surfaces are the (100) surface and (111) surfaces shown below in figure 2.[4] It can be seen that the (100) orientation displays flatter, square-like facets whereas the (111) orientation gives more triangular facets.

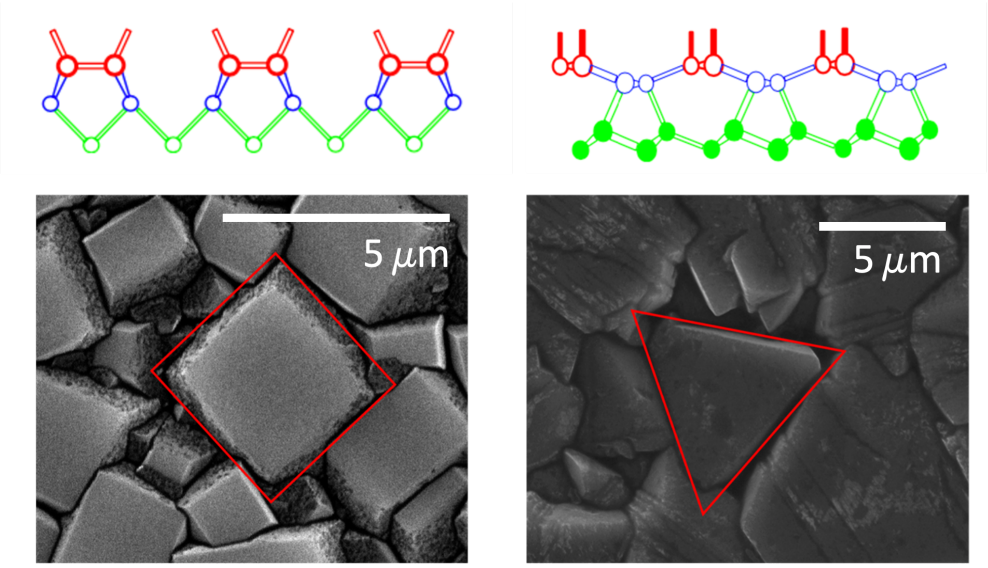

(a) (b)

Figure 2: *Crystallographic surfaces of diamond and associated SEM images of surface facets, a) the (100) surface contains two dangling bonds (usually terminated with hydrogen) per surface carbon atom however this often rearranges to form π bond dimers with other surface atoms as shown here in red, b) the (111) surface shows one dangling bond (red) per surface atom.*[4]

1.1.2 Types of diamond

Even before synthetic diamonds were available, diamonds needed a means of classification to represent their properties. In 1934 Robertson *et al.* distinguished between the two types of diamond based on infrared (IR) absorbance, ultraviolet (UV) absorbance, photoconductivity and optical effects - most notably birefringence, which is a property of a material that means its refractive index depends on the wavelength of incident light.[5] From these properties diamond could be classified as type I diamonds, which were opaque to UV light below about 300 nm, were poor photoconductors and showed birefringence, and type II diamonds which would transmit UV light, were good photoconductors and did not display birefringence.[6] In 1954 Sutherland *et al.* suggested that the properties associated with type I diamonds could be explained by the carbon atoms being in an abnormal state and the presence of impurities.[6] These impurities were shown to be nitrogen, which was present in type I but not type II diamonds. Further research allowed diamonds to be classified as type I (a or b) or type II (a or b) based on the impurities present and the structure of the crystal (figure 3).[7]

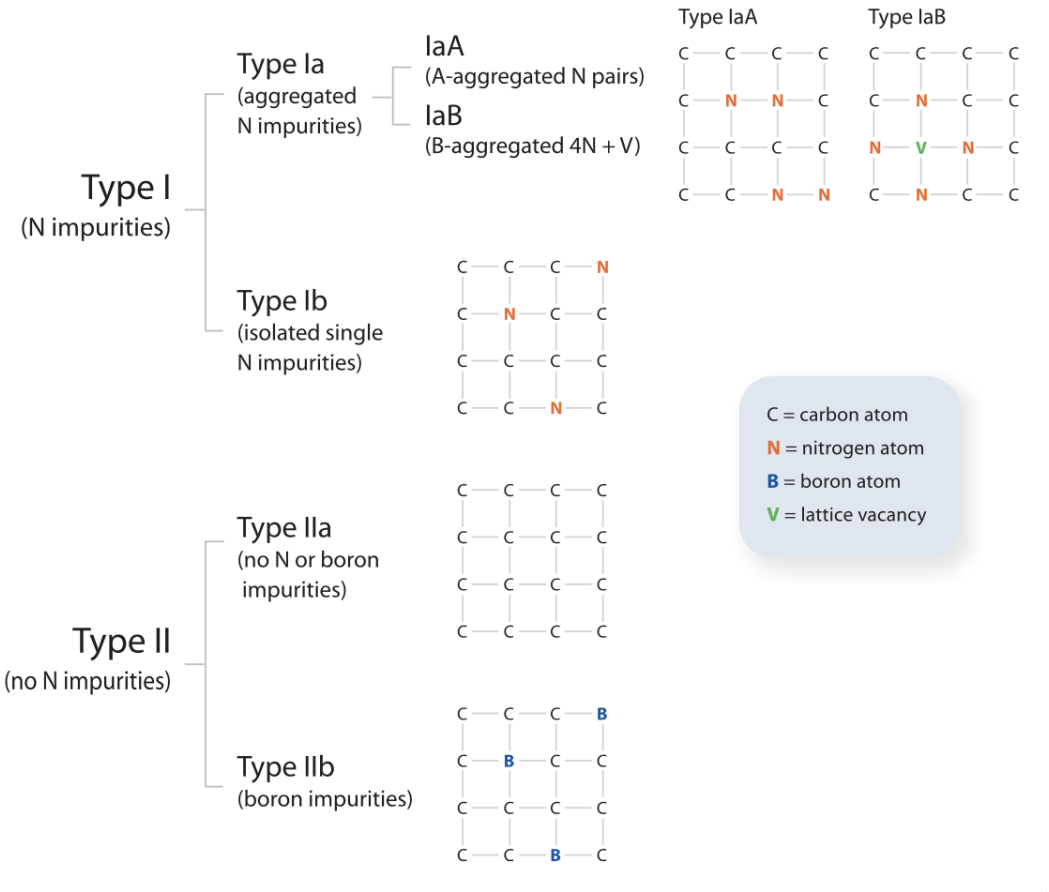

Figure 3: *Summary of the different types of diamond. From Breeding and Shigley.*[7]

1.2 Diamond growth

1.2.1 History

It is reported that the first synthetic diamonds were made in the 1950s by General Electric, using high-pressure high-temperature (HPHT) techniques, designed to replicate the way that diamonds are made in nature. However, these methods could not reliably produce diamonds which were large enough to be useful.[8]

The alternative to HPHT methods was to use gaseous substrates to add individual carbon atoms to a crystal.[8] This technique, now known as chemical vapour deposition (CVD), was first achieved by Eversole and although lots of research into these methods of growing synthetic diamonds was carried out in the 1950s, the first published papers did not appear until the late 1960s.[9,10] Derjaguin *et al.* showed that filamentary diamond crystals (otherwise known as whiskers, which are thin spiky crystals) could be grown onto diamond substrates using carbon-containing gases. However, they faced issues with the more stable graphite forming, which prevented further growth of the diamonds. The graphite had to be removed at

the end of the process which presented an extra challenge.[11] Poferl *et al.* then demonstrated that hydrogen (H_2) could be used to etch away 99.9% of the graphite left at the end of the process. They also showed that boron could be incorporated into the diamond crystal to form boron doped diamond (BDD), a p-type semiconductor (discussed later in section 1.3.2), by using a gaseous mixture containing 0.83% diborane (B_2H_6).[12]

A significant study by Spitsyn *et al.* in 1981 showed that for optimal growth, CVD should be carried out at reduced pressures and that the addition of H_2 in the gaseous mixture used to grow the diamond, prevented the formation of graphite. This paper also demonstrated that diamond could be grown on other substrates (heteroepitaxial), not simply diamond alone (homoepitaxial), which meant that the potential for synthetic diamonds to be grown on a useful scale was much more viable.[13]

1.2.2 Activation

CVD is now a very well established method for diamond growth. It involves activating a hydrocarbon and H_2 gas mixture which leads to the deposition of carbon atoms on a solid surface.[8,14] There are several ways of activating these gases but this report will focus on thermal activation using hot filaments and activation using a microwave plasma. Although not discussed in this report, other methods of activation are available including plasma jets, arch jets, welding torches and plasma torches.[8]

Hot filament CVD (HFCVD) involves activation of the gases using a hot filament within a vacuum chamber. The wires undergo resistive heating and metals such as tungsten or tantalum are typically chosen for the filaments due to their high melting points.[15] Growth of synthetic diamond onto non-diamond substrates by HFCVD was first reported by Matsumoto *et al.* in 1982. Hot tungsten filaments were used, in a chamber filled with hydrocarbon and H_2 gases, to deposit crystalline diamond onto silicon (Si) or molybdenum (Mo) substrates. The research found that as the methane (CH_4) concentration within the gas mixture increased from 0.5% to 2%, the shape of the crystals became more rounded and graphite peaks were detected in the Raman spectra. The effects of the temperature of the heater and filaments were also investigated and were shown to increase the growth rate. However, accurate measurements of the substrate temperature could not be obtained.[16] Figure 4 shows a typical HFCVD reactor.

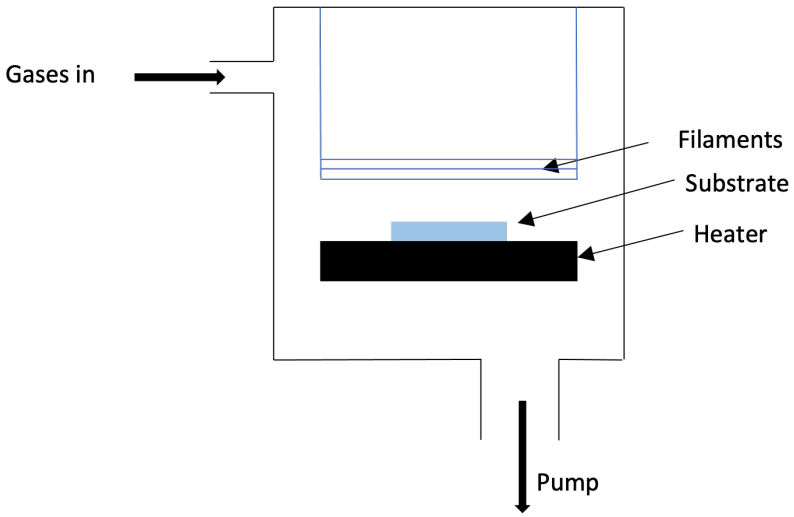

Figure 4: *Diagram showing the set-up of a typical HFCVD system.*

Microwave plasma CVD (MWPCVD) uses microwaves to supply energy to the the gas mixture causing the formation of reactive species. The electric field causes the electrons within the gaseous species (e.g H_2) to oscillate and they are accelerated out of the gas molecules. These electrons can then go on to collide with other molecules causing them to dissociate into reactive radicals.[17] One of the early examples of this technique was published by Kamo *et al.* in 1983.[8,18] With what was referred to as microwave glow discharge conditions, Kamo *et al.* successfully grew well defined diamond crystals that had not previously been achieved with plasma techniques.[18] MWPCVD techniques are now dominating synthetic diamond growth worldwide and a typical ASTEX-type reactor design is shown in figure 5.[8]

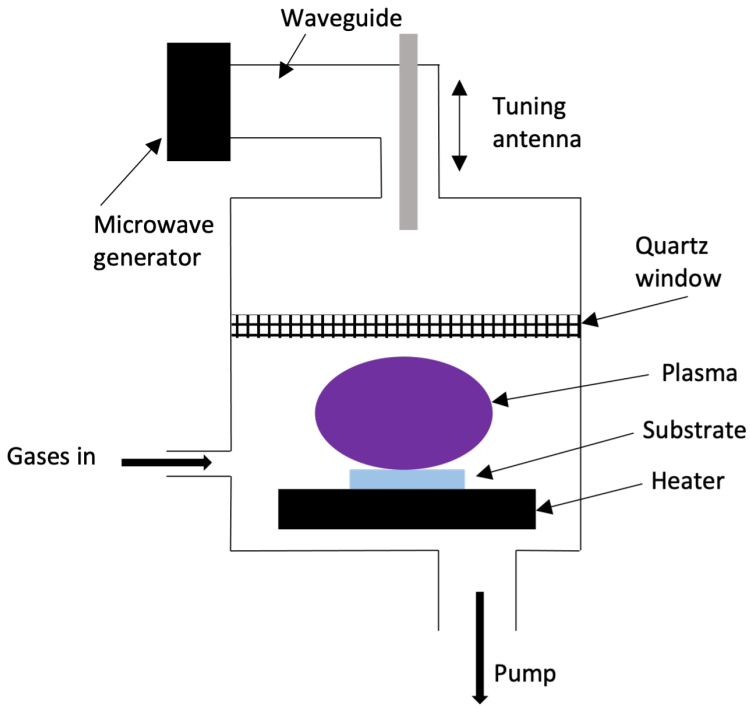

Figure 5: *Diagram showing a typical ASTEX-type MWPCVD reactor.*

1.2.3 Mechanism and gas composition

Activation of the gases (for example by hot filaments or plasmas) causes the formation of reactive radicals such as CH_3 or H which, when they strike the surface, can either adsorb or react. Figure 6a shows a schematic of this. H radicals are key to diamond growth because they can abstract H atoms from the surface, leaving reactive centres where additional carbons can attach (figure 6b).[8,14] Several independent crystals grow until they get close enough to form grain boundaries and continue to grow as a single film.[14] In general, substrates are seeded with diamond to start nucleation. Methods include using electrospray to spray the surface with nanodiamond, dip-seeding using a nanodiamond solution or even manual abrasion, where off-cuts of diamonds are used to scratch the surface of the substrate.

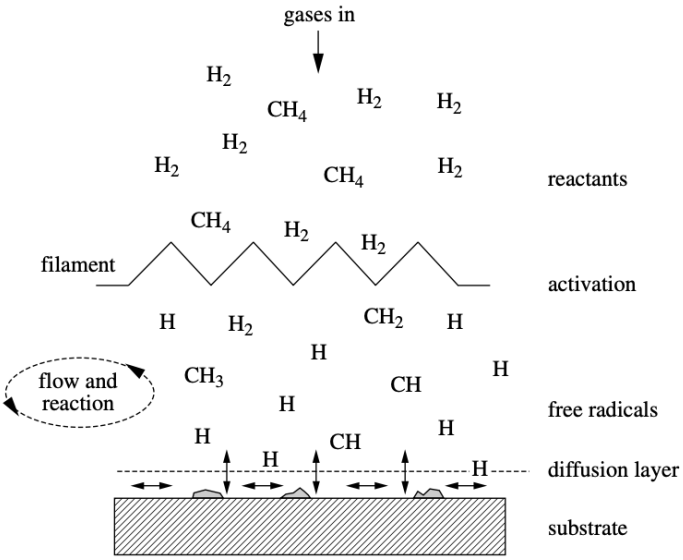

(a)

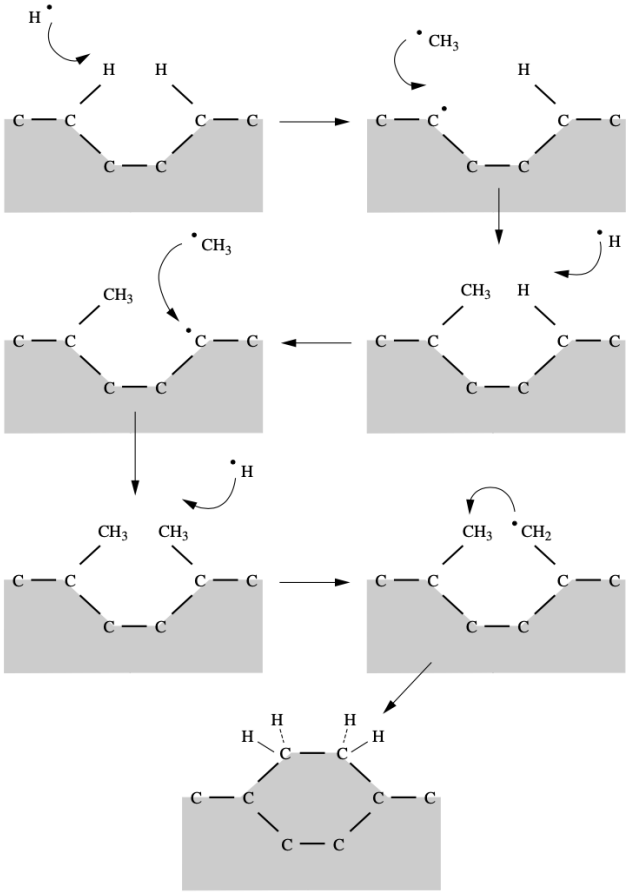

(b)

Figure 6: *Schematic of the physical and chemical processes involved in CVD, a) shows the overview of the gases, b) shows what is occurring at the surface. From May.*[8]

High proportions of H_2 and H radicals catalyse diamond growth and promote the growth of sp^3 diamond rather than sp^2 graphite.[8] The H radicals allow for the formation of reactive sites on the surface of the film and will etch sp^2 graphite carbons over sp^3 diamond carbons.[8,19] The proportion of CH_4 relative to H_2 plays a vital role in the quality and appearance of the diamond. Figure 7 shows a version of the Bachmann triangle, a phase diagram with the atomic fractions of H, C, and O atoms present on the axes, first produced by Bachmann *et al.* in 1991, using over 70 sets of experimental data.[20] It shows that diamond grown using low pressure conditions is only possible in a very small area of the phase diagram, which coincides with the CO tie line (running from the point at which CO occurs on the C-O axis, 0.5, to the opposite corner). Most CVD growths use a large excess of H_2 and no O_2, as shown in the bottom left region of the diagram. The effect of varying the CH_4 concentration, within this small area, will be investigated in this report.

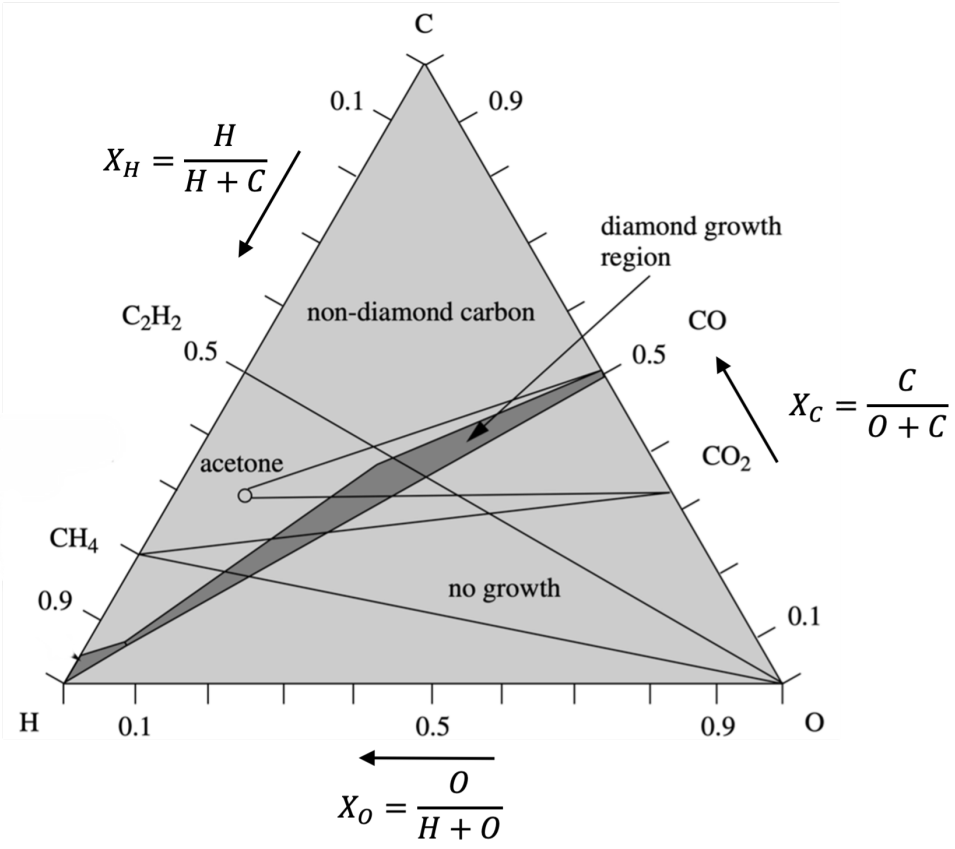

Figure 7: *Bachmann triangle showing C_H_O phase diagram for CVD diamond growth. Axes show the atomic fractions, X_a of each of the atoms within the mixture. Adapted from May.*[8]

1.2.4 Single crystals

Although methods of growing polycrystalline diamond are well established, single crystal diamond (SCD) grown using CVD methods is still a challenge. The growth of diamond on iridium (Ir) was first published in 1996 by Ohtsuka *et al.* and Ir is now considered to be the most effective substrate for SCD growth, due to dissolution of carbon into the bulk.[21–23] At low carbon concentrations, dissolution into the bulk is energetically favourable, however at high carbon concentrations (at or above $\sim$ 15% carbon) this process becomes unfavourable and carbon is driven up out of the bulk causing self-nucleation and fast diamond growth on the surface. This balance between the two processes is what makes Ir ideal for SCD growth. Other substrates do not show this fine balance. For example with Si, the dissolution of carbon into the bulk is not energetically favourable at any carbon concentrations, but with rhenium the dissolution into the bulk is still favourable at higher carbon concentrations. These two substrates do not lead to such effective SCD growth as they do not show a rapid expulsion of carbon to the surface, allowing for nucleation and growth.[22] Ir also shows a narrower distribution of orientations making SCD growth more likely.[23]

In order to achieve SCD growth, biased enhanced nucleation (BEN) is used.[24] This technique, first published as a predisposition process on Si substrates by Yugo *et al.* in 1991, used an initial nucleation step where the CH_4 fraction of the gases was increased by up to as much as 40% and a negative electric field was applied across the substrate surface (known as negative bias). After several minutes, normal CVD conditions were used for the remainder of the growth and very high densities of diamond nuclei were obtained after 5 minutes (10^{10} cm^{-2}). They showed that for Si substrates the minimum voltage required was -70 V and the minimum CH_4 fraction was 5 % for nucleation.[25] Ohtsuka *et al.* used this technique to grow diamond on Ir and found that an amorphous layer of carbon was formed on the substrate as a result of BEN and that the diffraction rings, due to randomly orientated crystals, were of very low intensity. Further studies were carried out to explain these findings.[21]

When BEN is used with Ir substrates, an amorphous layer of hydrocarbon initially covers the Ir, which is then bombarded by H radicals leading to etching of the hydrocarbon. An equilibrium between the deposition and etching is reached and a layer of amorphous carbon 1 nm thick is formed. Spontaneous nucleation of primary diamond nuclei can occur, although with a very low probability, so the number of nucleation sites is very small. New primary nuclei tend to form near the original nuclei, with similar orientations, creating crystal domains. BEN conditions cause the etching of diamond when grown on Ir, which means that the diamond crystals cannot grow vertically during the nucleation period. However, lateral expansion along the surface is possible, which leads to the formation of secondary diamond nuclei.[23,24,26] This growth arises through an orientated attachment (OA) growth mechanism which was explored by Li *et al.* and showed how the grain boundaries could be

eliminated.[26,27] They discovered that the particles continuously rotated until they matched the lattice precisely. Then, at distances of less than 1 nm, a "jump to contact" was observed, driven by short range forces that depended on orientation, which led to lateral growth by addition of single atoms.[27] Given that primary nucleation is very rare, the majority of nuclei would result from lateral growth from these primary nuclei. Once the BEN has been removed, the amorphous layer of hydrocarbon is etched away, leaving isolated crystalline diamond. This provides the nuclei for the SCD film to grow.[23,24,26] Figure 8 shows the steps involved in the nucleation of SCD on Ir using BEN.[23] BEN also helps to increase the amount of carbon that can be absorbed into the bulk, which when expelled, leads to rapid nucleation.[22] To date, Ir is the only suitable substrate with which BEN has successfully been used to grow SCD.[23,26]

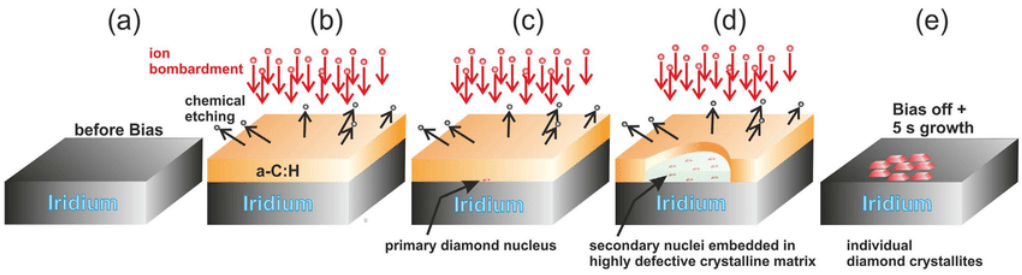

Figure 8: *Schema showing the steps involved in BEN on Ir, a) substrate before biasing, b) the amorphous carbon layer formed which is etched away by ion bombardment, c) spontaneous nucleation of primary diamond nuclei, d) lateral expansion of domains, leading to secondary nuclei, e) once BEN is removed, the amorphous layer is etched away leaving individual diamond crystals. From Schreck et al..*[23]

1.2.5 Analysis of diamond films using Raman spectroscopy

Raman Spectroscopy is a key technique used to identify and provide an indication of the quality of diamond films. A laser beam is used to probe the vibrational states of a molecule, similar to infrared (IR) spectroscopy. However, IR spectroscopy directly measures the energy difference between states by absorbing a photon (figure 9), whereas Raman spectroscopy involves the excitation of an electron to a virtual energy level by a photon of higher energy (visible light rather than IR), which then relaxes and emits a photon which can be detected. The difference between the absorbed and emitted photon is then used to determine the energy gap. Figure 9 highlights the three transitions normally observed in Raman spectroscopy; Rayleigh (R) scattering where the electron relaxes to the same energy level at which it started, Stokes (S) scattering where the electron relaxes to a higher energy level than the level at which it started and anti-Stokes (A) scattering where the electron relaxes to a lower energy level than the level at which it started.[28]

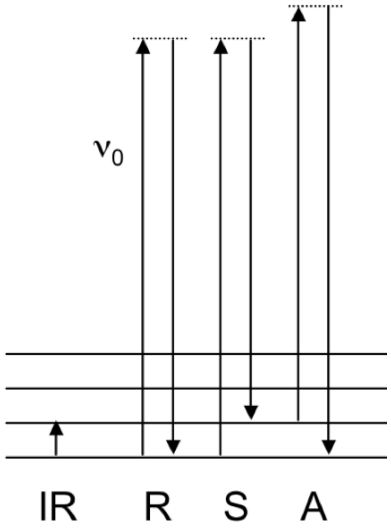

Figure 9: *Scheme showing the energy changes occurring in IR and Raman spectroscopy. Rayleigh (R), Stokes (S), and anti-Stokes (A) Raman transitions are shown separately. From Sanzenbacher.*[28]

The Raman spectrum of SCD shows one sharp peak at 1332 cm^{-1}, due to the vibrations of the sp^3 structure (figure 10a). Figure 10b shows the Raman spectrum of graphite, where two different sp^2 vibrations can be detected; named the D peak and the G peak. Polycrystalline diamond often contains peaks from both sp^3 and sp^2 carbons. The presence of a large G peak in a diamond Raman spectrum can indicate a low-quality diamond, which is illustrated by figure 11.

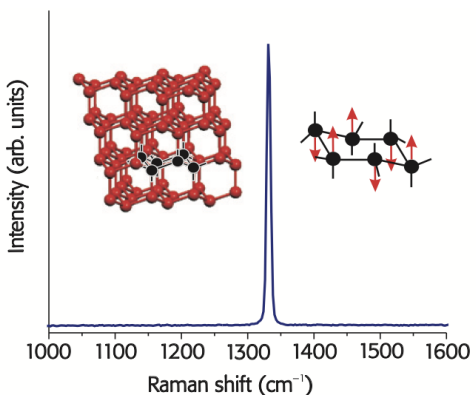

(a) Diamond

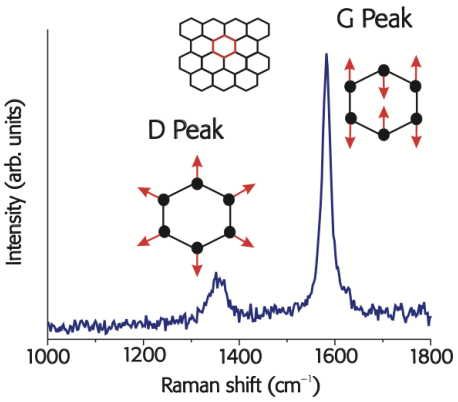

(b) Graphite

Figure 10: *Raman spectra of a) SCD and b) graphite. From Sanzenbacher.*[28]

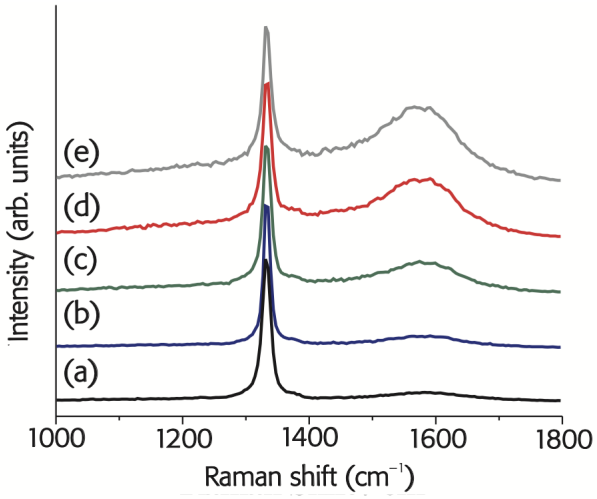

Figure 11: *Graph showing the increasing intensity of the G peak (from a to e) indicating a decrease in diamond quality. From Sanzenbacher.*[28]

1.3 Diamond as a semiconductor

1.3.1 Band theory

Band theory underpins our understanding of the electronic properties of solids. When molecules crystallise to form a solid, the overlap of a large number of atomic orbitals (AOs) leads to a series of closely spaced molecular orbitals (MOs). These can be thought of as a continuous band with the most bonding character at the bottom and the most antibonding character at the top (figure 12a). A density of states diagram (figure 12b) can be built up, taking the number of energy levels in a set range, divided by the width of the range, to calculate the density of states (ρ) at any given point. This is not uniform across the whole band as some energy levels are closer than others. Each set of AOs generates a band (for example overlap of s orbitals would lead to an s band) and multiple bands separated by band gaps (figure 12c) build up the electronic structure.[29]

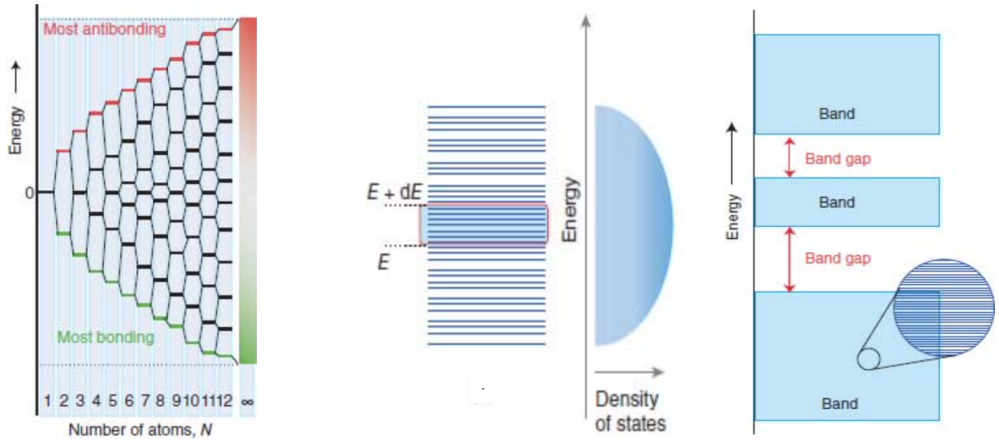

(a) (b) (c)

Figure 12: *Summary of how electronic structure of solids is built up, a) energy level diagram to show how multiple AOs can overlap to form a continuous band which leads to a density of states diagram, b) density of states diagram showing the number of energy levels in an infinitesimal range, c) overlap of different AOs leads to the formation of several bands separated by band gaps.*[29]

The Fermi level is defined as the highest occupied energy level at T = 0 K and allows materials to be categorised as conductors or insulators. As shown in figure 13, the Fermi level of conductors (typically metals) lies within a band and the Fermi level of insulators lies between bands. In metals the highest occupied band is only half full so electrons can easily be promoted to the next energy level within the band, therefore the electrons are classed as mobile, and the material can conduct (figure 13a). The conductivity of metals decreases with temperature. Insulators on the other hand have a filled band (valance band) and an empty band (conduction band) with the Fermi level between them, which means that electrons cannot be easily promoted so are not mobile (figure 13b).

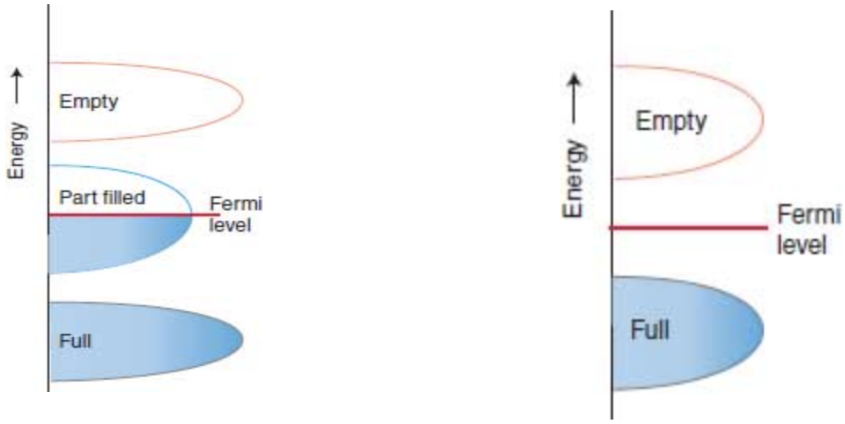

(a) Conductor (Metal) (b) Insulator

Figure 13: *Diagrams to show band structure and Fermi level of a) a metallic conductor and b) an insulator.*[29]

There is a third class of compounds, known as semiconductors, which can be divided into intrinsic and extrinsic semiconductors. Intrinsic semiconductors occur in materials with very small band gaps where a small amount of thermal energy can cause electrons to move into the conduction band (figure 14a). This also leaves positive holes within the valance band. The presence of both the holes and promoted electrons (now mobile) causes the material to become conductive and the conductivity increases with temperature as more electrons get promoted to the conduction band. It is worth noting that at room temperature most semiconductors have a much lower conductivity than metallic conductors because fewer electrons and holes are free to move. The second type of semiconductors, extrinsic, are semiconductors due to the presence of small amounts of impurities.[29]

Extrinsic semiconductors can be broken down into two classes: n-type and p-type. The addition of atoms with more electrons than the parent atom, leads to n-type doping whereas addition of atoms with fewer electrons than the parent atoms leads to p-type doping. With n-type doping the filled dopant band lies near the empty conduction band (figure 14b), which allows the electrons to move up into the conduction band and move through the crystal. P-type doping forms an empty acceptor band just above the valance band (figure 14c), which can accept electrons and form holes within the valance band allowing the electrons to move. The “n” and “p” labels are based on whether the charge carriers are negative electrons or positive holes respectively.[29]

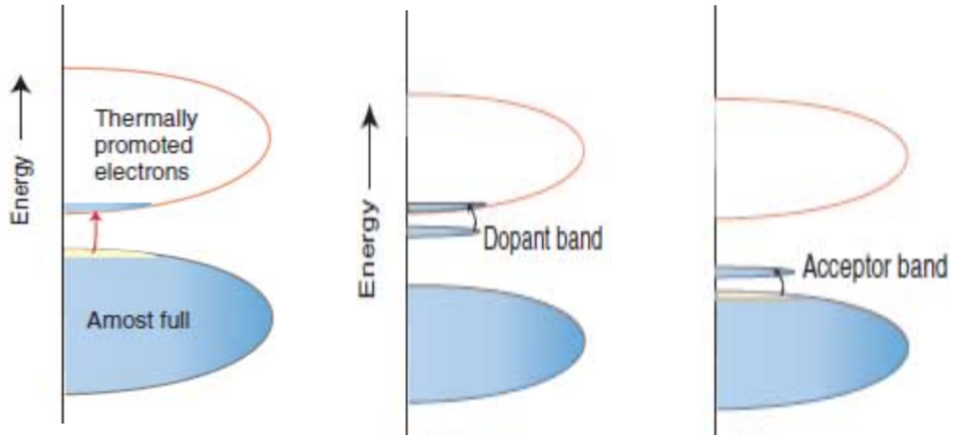

(a) Intrinsic (b) n-type (c) p-type

Figure 14: *Diagrams to show band structures of semiconductors, a) shows an intrinsic semiconductor with a narrow band gap. The electrons have been promoted to allow for the formation of both positive and negative charge carriers, b) an n-type extrinsic semiconductor showing the dopant band just below the conduction band, c) a p-type extrinsic semiconductor with the acceptor band just above the valance band.*[29]

1.3.2 Diamond doping

Intrinsic diamond is a wide bandgap insulating material (band gap 5.47 eV), however the addition of dopants can cause changes to the conductivity as described above.[30] Various dopants have been used throughout the years and although doped diamond can be formed *via* ion-implantation, adding the dopant into a gas-mixture in CVD techniques is the most well established technique and avoids the risk of damaging the crystal. Boron doped diamond (BDD) is by far the most common dopant for semiconducting applications and exhibits p-type doping.[31] Although n-type doping, for example using phosphorus, has been achieved and is often required for more complicated electrical devices, it is much harder to achieve and will not be discussed any further in this report.[32]

The conductivity of BDD can be carefully controlled by the amount of boron present in the crystal. One of the most common uses of BDD is as inert electrodes in electrochemistry and it has even been shown to exhibit properties that surpass metals such as platinum. Other electronic devices such as temperature or pressure sensors and Schottky devices have also used BDD.[31] The use of BDD in diamond detectors is also becoming more and more popular.[33]

The presence of boron in the diamond can also cause changes to the appearance of the Raman spectrum. BDD causes a red-shift (the peak moves to a lower wavenumber) in the diamond peak and a peak broadening. Two broad peaks are also observed at 500 cm^{-1} and

1200 cm^{-1}. Figure 15 shows the Raman spectra, between 1000 cm^{-1} and 1500 cm^{-1}, of samples containing different amounts of boron doping. As the boron concentration increases the peaks become broader and more red-shifted. The width and position of the peaks can be used to determine the boron concentration of samples if a suitable set of calibration data is available.[34]

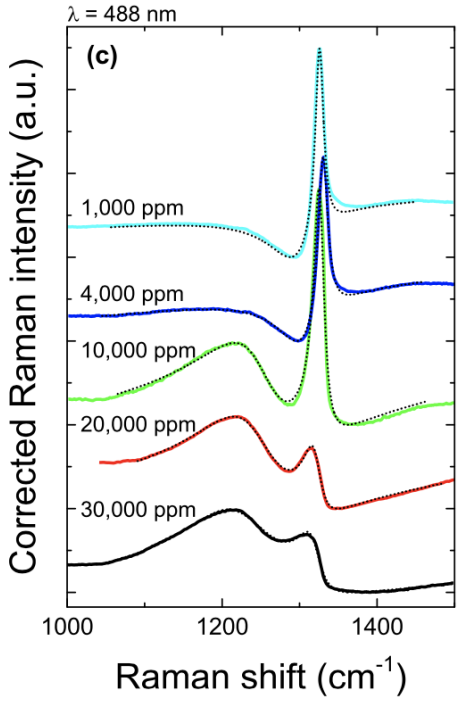

Figure 15: *Raman spectra of BDD containing different levels of boron doping. From Mortet.*[34]

1.4 Diamond detectors

1.4.1 Theory

As mentioned above, diamond possesses many properties that make it effective for radiation detection. Its radiation hardness and chemical inertness mean diamond is suited to extremely harsh environments which other elements such as Si cannot withstand. The high resistivity and large band gap of diamond are also useful properties.[35] In theory, any radiation with a higher energy than diamond's band gap (5.47 eV) can be detected, including various particles such as alpha particles, electrons or neutrons.[36] The basic concept of diamond detectors is that radiation, for example an electron, is fired at a diamond crystal, causing secondary electrons to be released along with the formation of positive ions or "holes". An electric field is applied to the device causing the electrons to move towards the positive electrode and the holes to move towards the negative electrode. These can both be detected by the presence of a current (figure 16).[36–38] Anything that causes the formation of electrons and holes within

the crystal can be detected.[35] These devices can run in pulse counting mode where each individual event can be detected or current mode where a continuous signal is seen.[36]

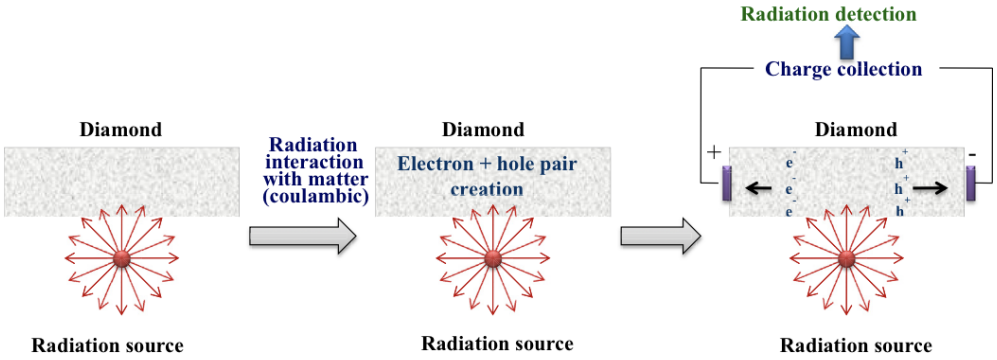

Figure 16: *Schematic showing the basics of how a diamond radiation detector works. From Jain et al..*[36]

One of the difficulties with diamond-based detectors is the poor resolution that is achieved with polycrystalline diamonds. The presence of grain boundaries or defects within the crystal can cause the pairs of holes and electrons to become trapped and then they cannot be detected. This means that SCDs are required for high resolution diamond detectors which, as described in section 1.2.4, are difficult to grow.[36]

1.4.2 History

The use of diamonds as detectors can be traced back to the 1920s when research was carried out into natural diamonds as photoconductive UV detectors which acted as crystal counters to replace the traditional gas counters.[35] In 1949 Hofstanter published a review paper on "crystal counters" followed by a second paper in 1950 which detailed how basic radiation detectors worked.[37,38] At a similar time, Friedman *et al.* showed that only type II diamonds (transparent to UV radiation) demonstrated the properties required for detectors.[39,40] Freeman *et al.* studied this further and used birefringence experiments to show that the presence of laminations (lines that show up in birefringence patterns due to areas of different symmetry) can affect the detector properties. These laminations were caused by a mosaic-like structure, a feature of non-counting diamonds, whereas in counting crystals fewer laminations were observed. Their explanation was that the mosaic-like structure prevented electrons from passing through the crystal.[40,41] These low birefringence type II diamonds are now classed as type IIa diamonds meaning they contain no impurities.[7]

Various groups have published work looking at the energies associated with the formation of ions and holes within the crystal, when diamond is used as a detector. In 1950 McKay showed that the movement of the charged species could be quantified and Champion and Wright published their work in 1958 looking at alpha particles and diamond counters. They

noted that recombination is often observed between the charged species and they studied the energy of such processes.[42,43] In 1959 Kennedy used pulse counting methods to detect electrons and these techniques were also used to measure the energy of the ion pairs forming within the diamond.[44] Dean and Male also studied the energies associated with the formation of holes and presented an explanation for the difference in measurements between alpha particles and electrons (the difference is caused by the different magnitudes of the electric fields produced by the particles themselves along their path within the crystal). They reported a minimum value for the mean energy required to create an electron hole pair from an alpha particle as 24.5 ± 1 eV and the value for the electrons reported by Kennedy was 18.5 ± 1.5 eV.[44,45] There has also been a myriad of other work done exploring the use of diamonds as detectors and particle counters and their interactions with, for example, x-rays and gamma rays. Kania *et al.* published a review paper in 1993 which describes this work in more detail.[35]

1.4.3 Designs

There are various designs used within the field of diamond detectors, some with intrinsic undoped diamond and some with doped p-type semiconducting diamond. One of the simplest designs, using intrinsic diamond, is known as a metal-insulator-metal (MIM) device. It consists of a high resistance diamond between two metal contacts (electrodes) with a voltage applied across the device. When the electron and hole pairs are formed, they move towards the electrodes and a current is detected.[35] Other designs include various semiconductor junctions where the semiconducting diamond is in close contact with a metal, another semiconductor or even intrinsic diamond. Semiconductor-metal contacts form what are known as Schottky barriers or Ohmic junctions (depending on the level of doping) where the diamond and metal come into contact with one another.[46] Schottky barriers, or rectifying contacts, are associated with low level doping and only allow current to flow in one direction (figure 17a). Ohmic contacts on the other hand, are associated with higher levels of doping and allow current to flow in both directions (figure 17b).[46,47] Metal-semiconductor-metal devices require an external voltage to be applied due to the symmetry of the contacts whereas other detectors that simply have one Schottky junction, have an internal in-built electric field, so do not require an external voltage. An example of this is a p-type-insulator-metal (PIM) device, in which an intrinsic layer is introduced to increase the thickness of the region containing the built-in field allowing more electron carriers to be collected.[48]

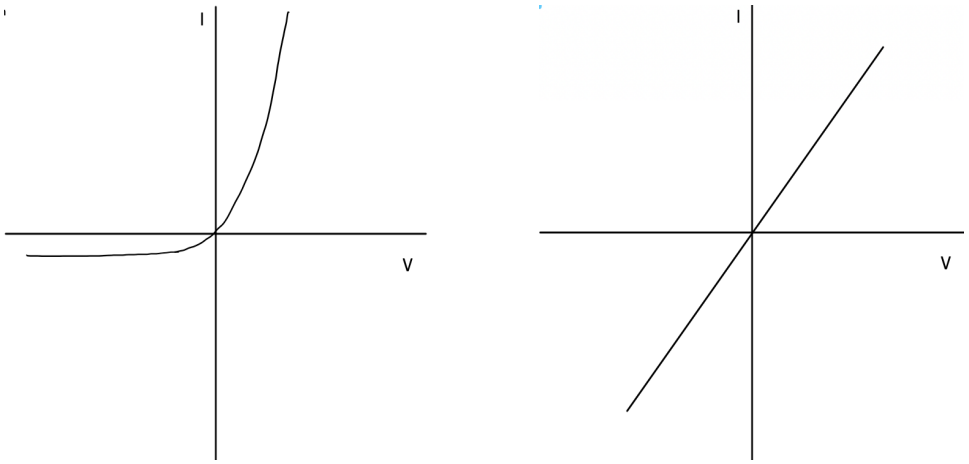

(a) Schottky Junction (b) Ohmic Contact

Figure 17: *Graphs showing current (I) voltage (V) curves for a) a Schottky junction where current can only flow in one direction and b) an Ohmic contact where current can flow in both directions.*

An example of another detector design was published by Verona in 2011. This device uses a PIM design which has a Schottky junction between the metal and the intrinsic diamond. The I-V curves for this design demonstrated this Schottky behaviour (figure 18). These devices showed very low background noise meaning the signals from the incident radiation could be clearly detected.[49]

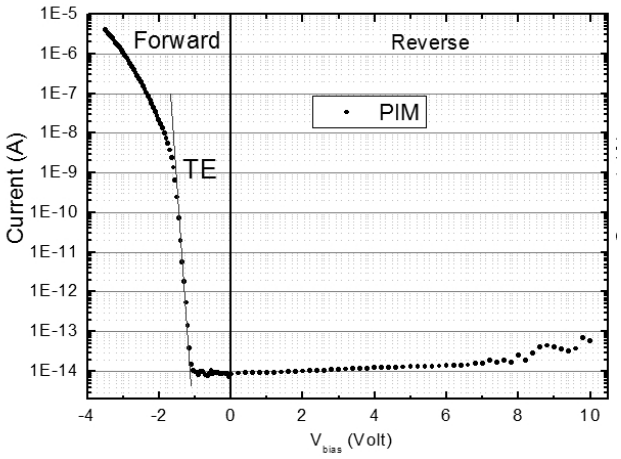

Figure 18: *Graph showing the I-V curve for a PIM device.*[49]

1.4.4 Charge collection efficiency

One of the measures of the effectiveness of a detector is the charge collection efficiency (CCE) η_c. The CCE is the fraction of the initial charge that ends up being detected, i.e. the charge detected compared to the charge produced within the crystal, due to incident

radiation or ions.[50,51] It is often used as a way of evaluating detectors and is described by equation 1, where Q_{exp} is the experimentally measured charge and Q_{gen} is the amount of charge generated in the diamond crystal during the experiment.

$$\eta_c = \frac{Q_{exp}}{Q_{gen}} \tag{1}$$

An example of CCE values in use was published by Sato *et al.* in 2016. They used CCE values to compare the detection of various charged particles by a SCD CVD detector. The detector was a simple MIM design with aluminium (Al) and gold (Au) metal contacts. The results demonstrated a 95% or more CCE for He^+ ions, however much lower CCE values for heavier atoms, such as Au, which had a CCE of $\sim$ 30%.[51]

1.4.5 Recent work

Research is ongoing into the use of diamonds as detectors within a variety of industries and a few examples of some of the most recent detection devices are given below. Lioliou *et al.* recently published a study using SCD with Al contacts as a detector for low energy x-rays and electrons. However, the CCE values were relatively low at $\sim$ 15-20%. They hypothesised that these low values were caused by the presence of a depletion region (at the interface between the metal and the insulator is a region where no charged species are present), which reduced the applied electric field. With further refinement these CCE values could be improved.[52]

Following on from Lioliou's research, a paper was published investigating the use of CVD SCD in electron spectrometers, with a particular focus on their use in space and potential space science instruments. Currently, solid state detectors made from Si need to be kept below 20°C and often require shielding from radiation. Diamond could be the solution to these issues. An MIM detector with silver electrodes was used to detect relatively low energy electrons ($\leq$ 63 keV) however there were some issues with the device becoming polarised. They were unable to explain the exact cause of the polarisation, so further work is required, but there is potential for these devices to have very high quantum efficiencies (amount of energy deposited in the detector by the electrons hitting the face of the detector, as a function of the electron's energy). With electron energies of 66 keV they achieved a quantum efficiency of 0.79 but with the potential to increase to 0.97 by reducing polarisation effects.[53]

Su *et al.* used an MIM design with SCD between two Au electrodes. The structure is shown in figure 19. This device was able to detect alpha particles and gamma radiation and gave extremely high CCE values of $\sim$ 99%. The device was also shown to respond quickly and was suitable for fast-timing applications.[33]

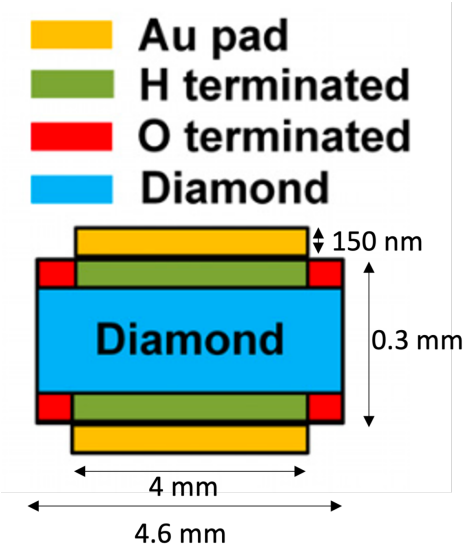

Figure 19: *Structure of MIM diamond detector reported by Su.*[33]

Curtoni *et al.* have been researching the use of CVD diamond detectors in hadrontherapy. Hadrontherapy is a type of radiotherapy based on ion beams, however it is difficult to accurately measure the ion range within the patient. They have been investigating the use of diamond detectors in an ion range verification system, and have had some success, especially with CVD SCD, which can count numbers of individual protons within a cluster. However, polycrystalline detectors were also tested and despite lower resolutions than the SCD detectors, they showed good results when using carbon ion therapies.[54]

Despite lots of recent success within the field of diamond detectors there are still issues surrounding polarisation effects or lack of current due to depletion regions (space-charge effects). Abubakr *et al.* have published a paper using laser processing of the diamond surfaces within a diamond detector which helps to selectively dope regions of the diamond and can help to improve the metal-diamond contact. In turn, this has been shown to reduce space-charge effects and increase CCE values. The diamond was submerged in a liquid containing the dopant (for example phosphoric acid was used to dope with phosphorus) before shining a laser beam onto the sample at the site where doping was required. This technique has the potential to improve detectors that are, for example, used in radiotherapies such as those mentioned above. Figure 20 shows the improvement to the current density measurements, and therefore sensitivity of the laser processed contacts, compared to typical metal contacts, such as Ti or Mo.[55]

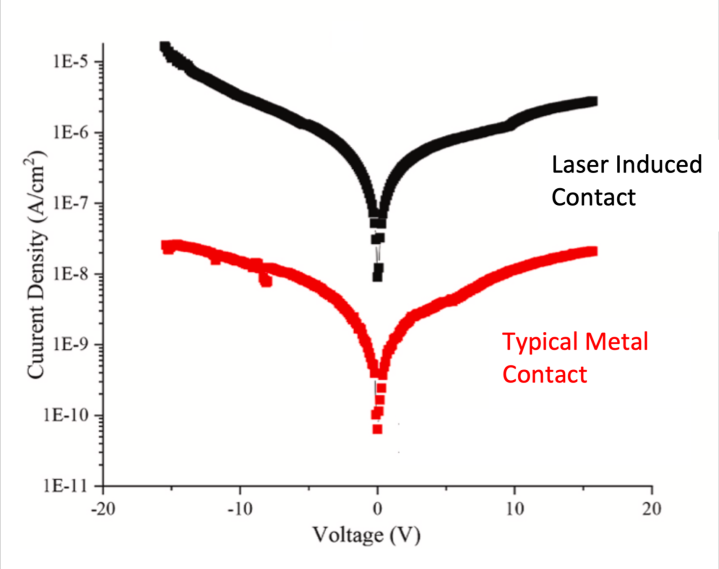

Figure 20: *Graph showing improved sensitivity of laser processed contact compared to a typical metal contact. From Abubakr.*[55]

1.5 Tritium detection

1.5.1 Tritium decay

Hydrogen has three isotopes; ^{1}H is the most common however ^{2}H (deutirium) and ^{3}H (tritium) play an important role as fuel in fusion reactors. Tritium and deuterium come together to form helium-4 and a neutron, releasing high amounts of energy (2). However, tritium is not naturally abundant, therefore must be produced from various lithium-based materials such as Li_2TiO_3, by bombardment with neutrons. One of the issues in fusion reactors is that hydrogen and its isotopes can penetrate the metal walls within the reactor and are retained. The result is that the amount of available fuel decreases, so it is vital to be able to detect that there is enough tritium available for the reaction.[56] Due to the radioactive nature of tritium it is also important to ensure that any tritium which escapes into the environment can be detected.

$$^{3}_{1}\mathrm{H} + ^{2}_{1}\mathrm{H} \longrightarrow ^{4}_{2}\mathrm{He} + ^{1}_{0}\mathrm{n} \tag{2}$$

Tritium decays by beta decay into helium-3, a beta particle (electron) and a neutral subatomic particle called an antineutrino (3). However, unlike a lot of beta decay paths, the electron is very low energy with an average of 5.7 keV rather than a few hundred keV (figure 21). The total energy of the electron and antineutrino is 18 keV. Tritium also has a relatively short radioactive half-life of 12.3 years and an extremely short biological half-life of 10 years, which means that if ingested, only 1 in 650 tritium particles will decay whilst in the body. So, while tritium is considered highly radioactive, it has very low radiotoxicity.[57]

$$^{3}_{1}\mathrm{H} \longrightarrow {}^{3}_{2}\mathrm{He} + \mathrm{e}^{-} + \bar{\nu} \tag{3}$$

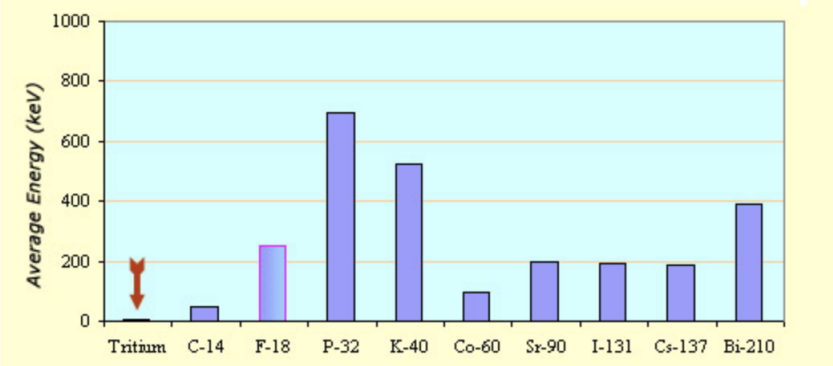

Figure 21: *Average energy of radioactive isotope decay paths for several different species including tritium.*[57]

1.5.2 Current detection methods

Due to the very small size of hydrogen and its isotopes, some of the common detection techniques, such as x-ray photoelectron, are not suitable for measuring tritium. The beta decay path, described above in section 1.5.1, allows for the detection of tritium using radiation detectors. However, the very low energies of the emitted electron mean this decay is very hard to detect due to its low penetration.[58] One of the most common ways to detect tritium is liquid scintillation counting (LSC). This technique involves mixing the tritium with a scintillation cocktail (liquid) which normally contains a solvent and a compound that will undergo luminescence (scintillator). The energy from the decay is absorbed by the solvent and transmitted to the scintillator and photons are emitted which can be detected. However, this method requires the tritium to be in liquid form therefore cannot be used in real-time, as samples of the gas must be taken rather than using continuous measurements. The other disadvantage is that only one isotope can be present in the sample.[58,59]

A common way to detect tritium in the gas phase is to use ionisation chambers that detect the electrons emitted as a current (figure 22). The tritium can be injected directly from a gas line and the larger the volume, the more accurate the measurement. The other common way to measure gaseous tritium is to use proportional counters. This involves mixing the tritium with another gas (counting gas) which becomes ionised when the tritium decays. The electrons released can therefore be detected, but this method is unsuitable to use with gas lines because the additional counting gas must be added to the original gases.[59]

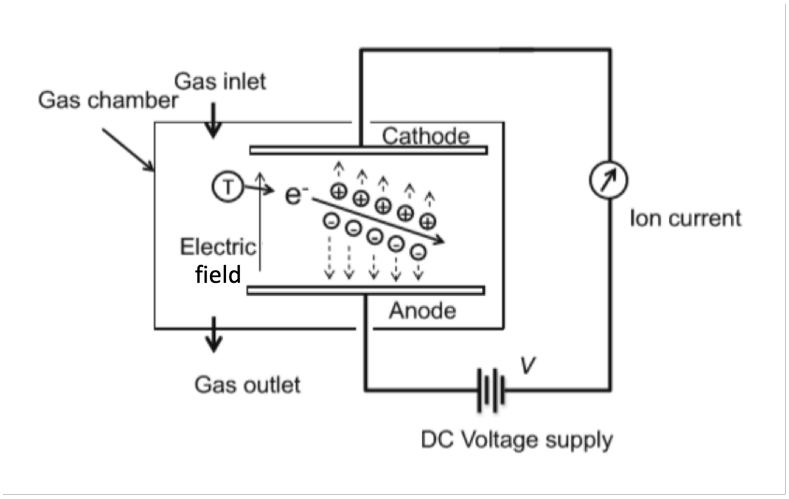

Figure 22: *Diagram of ionisation chamber. From Fichet*.[59]

Despite these common detection methods, suitable real-time measurements of tritium within the pipes of fusion reactors are difficult. Some recent papers have published possible solutions however there is still no perfect solution. O'hira *et al.* have developed a technique to detect tritium in fusion reactors using Raman spectroscopy. The device is non-destructive and can be used in real-time to accurately account for not only the amount of tritium but also the amount of deuterium and H_2. However, this device can only be used for individual gas lines not mixtures of gases as the tritium cannot be accurately distinguished.[60]

Jang *et al.* published a study using optical fibres as radiation detectors for tritium. They used a scintillator to generate photons that are passed through the optical fibres to a photo-detector. Although further modifications are required to improve the efficiency and to get real-time measurements the basic principle has been shown to work and shows promising results.[58]

1.6 Aims

As discussed in section 1.5.2, real-time detection of tritium in fusion reactors is still an issue to be resolved. Without accurate knowledge of the amount of tritium and therefore fuel in the rectors, the process cannot reach maximum efficiency and the safety implications of not being able to detect tritium could be severe. The long-established effectiveness of diamond in detecting radiation (as described in section 1.4), coupled with its other unique properties (such as being chemically inert), lend itself to coping with the harsh conditions of a fusion reactor and suggest that diamond could be the ideal material for detecting radiation emitting from tritium in fusion reactors.

As previously discussed, the best diamond-based detectors use SCD, as the presence of grain boundaries can lead to the trapping of the electron and hole pairs. However, BEN,

which is required to grow SCD in a MWPCVD reactor, was not possible with the equipment available. Therefore, conditions which were likely to form the largest crystals, and hence the fewest grain boundaries, were investigated instead. The aim of this project was to optimise the conditions for growth of large grains of CVD diamond, first on Si and then on Ir on yttria-stabilised zirconia (YSZ). The conditions were chosen to emulate SCD growth conditions. The objective was then to use the films to fabricate devices that could be used as potential tritium detectors, with first Al and then graphene top contacts. The first goal was a metal-insulator-metal (MIM) design grown using MWPCVD and then a p-type-insulator-metal (PIM) type design, using the HFCVD reactors for the boron-doped p-type layer. Raman and scanning electron microscopy (SEM) images were used to characterise the diamond films.

2 Results and discussion

2.1 Optimisation of conditions for silicon

In order to optimise the conditions for Ir substrates in the MWPCVD system, 12 Si substrates were tested using a range of conditions based on SCD growth. A range of different pressures and CH_4 concentrations were investigated whilst keeping the total flow rate (600 sccm) and input microwave power (1200 W) constant. Due to equipment limitations, a total flow rate of 600 sccm was chosen to allow for the full range of CH_4 concentrations. Exploring the conditions used in literature sources, values ranging between extremes for previous SCD growth were used in this experiment and are shown in table 1. The chosen limits for CH_4 concentrations were based on a recent paper by Arnault *et al.* who noted that at the lower limit of 1% CH_4, etching was seen and the highest growth rates were achieved at 13% CH_4.[61] The values chosen in between these limits gave a good spread of results. They also speculated that high pressures would lead to higher growth rates however Linnik *et al.* favoured much lower pressure ($\sim$ 20-30 torr (1 torr = 133 Pa)) which were also used by Schreck *et al.*.[23,62] A high pressure limit of 250 torr was chosen to ensure the power supply was still sufficient. A low pressure limit of 50 torr was chosen, slightly above those used in these studies to try and avoid the effects of etching due to pressure being too low. The middle pressure, 120 torr, was used as this was the standard pressure used in the MWPCVD reactor. All samples and associated conditions are listed in tables in the supplementary information along with all SEM images and Raman data.

Pressure / CH_4 %	**50 torr**	**120 torr**	**250 torr**
1 % **(6 sccm)**	Sample Si_6 0.2 mm spiral T = 720 °C	Sample Si_7 0.2 mm spiral T = 1050 °C	Sample Si_8 0.1 mm wire T = 1050 °C
4 % **(24 sccm)**	Sample Si_11 0.2 mm spiral T = 700 °C	Sample Si_10 0.2 mm spiral T = 1050 °C	Sample Si_9 0.1 mm wire T = 1000 °C
10 % **(60 sccm)**	Sample Si_12 0.25 mm spiral T = 790 °C	Sample Si_13 0.2 mm spiral T = 1050 °C	Sample Si_14 0.1 mm wire T = 1000 °C
13 % **(78 sccm)**	Sample Si_15 0.25 mm spiral T = 770 °C	Sample Si_16 0.2 mm spiral T = 1070 °C	Sample Si_17 0.1 mm wire T = 1050 °C

Table 1: *12 MWPCVD runs to optimise growth conditions for large grains. All done at a power of 1200 W and total flow rate of 600 sccm. The spacer wire used is indicated along with the initial temperature. All runs were three hours long. 1 torr = 133 Pa.*

SEM images revealed a huge variety of grain size and shape across the sample set. The average grain size was measured by taking an average of 10 randomly chosen grains and the thickness was measured. A plot of the average grain size vs thickness is shown in figure 23, which shows the average grain size increasing with thickness before levelling off once the film is thicker than ~ 15 μm. From the graph alone it appears that sample Si_9 may be the best candidate however this sample, done at high pressure (250 torr), was found to be very non-uniform; it contained some very large grains and many small grains (figure 24). Given that the aim was a reproducible set of conditions, that reliably gave large polycrystalline grains, it was decided not to pursue the conditions used for sample Si_9 any further.

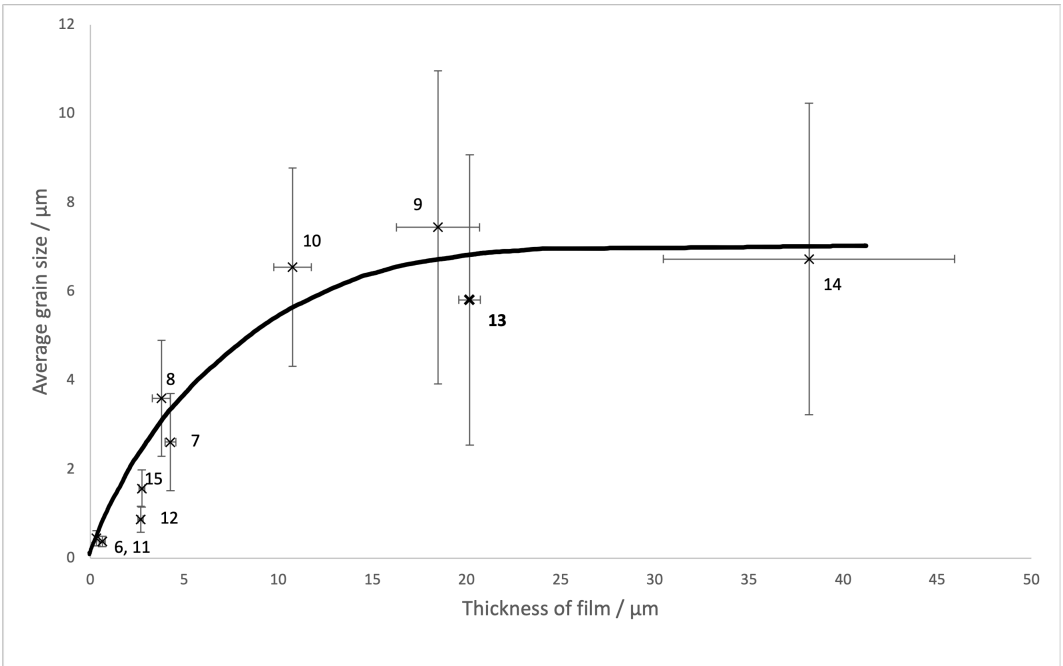

Figure 23: *Graph to show average grain size against thickness for the 12 Si samples grown using MWPCVD. Samples 16 and 17 did not show any significant crystals due to their graphitic nature so were omitted from the graph. Trend line shows an increase in grain size with thickness before leveling of once the thickness exceeds ∼ 15 µm. Error bars show standard deviations.*

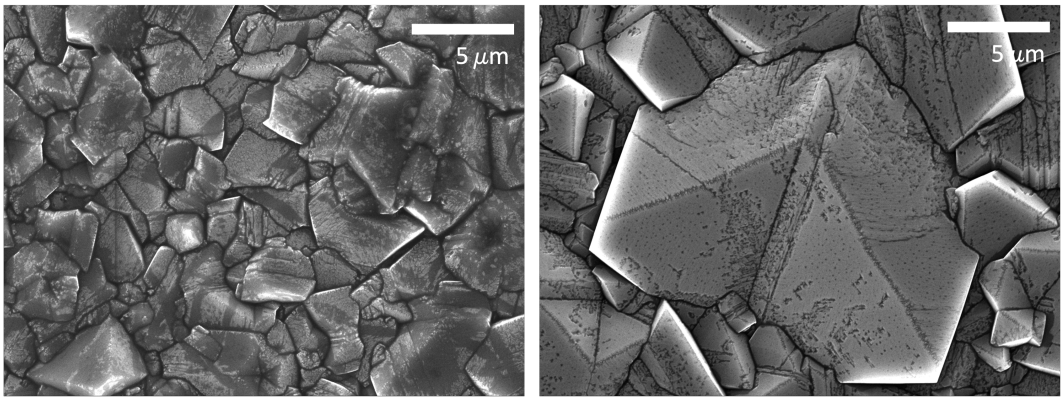

Figure 24: *SEM images of the variation in grain size of sample Si_9.*

Non-uniformity was found within all the high pressure samples and therefore the high pressure conditions were not investigated any further. Similarly, the low pressure conditions were also excluded based on very small grain sizes and slow growth rates. The low (1%) and high (13%) CH_4 concentrations also provided unsatisfactory grain sizes so they were excluded. Notably, samples 16 and 17, despite high growth rates, were extremely graphitic and showed no obvious diamond crystals which could be measured, so are not shown in

figure 23. It is likely the 13% CH_4 conditions are outside the range of diamond growth shown by the Bachmann triangle (figure 7) as discussed in section 1.2.3.

The remaining samples, Si_10 and Si_13, were similar in terms of grain size (given the high levels of inaccuracy associated with choosing grains at random), yet sample Si_13 gave almost double the growth rate (in three hours, sample Si_10 grew $\sim 11\ \mu$m whereas sample Si_13 grew $\sim 20\ \mu$m). Both Raman spectra (figure 25) showed good diamond peaks with sufficiently small G and D bands, however the most significant factor was the highly uniform (100) crystals formed with the conditions used for sample Si_13 (figure 26). Sample Si_10 (figure 27) was less uniform and showed no obvious preference for (100) or (111) orientation. This fits well with the study done by Zhang *et al.*, who determined that the ratio of the reactive radicals $[C_2H_2]/[CH_3]$ determined the orientation of the diamonds. As the CH_4 concentration increases, so does the ratio and the growth shifts from (111) facets to (100) facets. This is because the growth of (100) facets depends on CH_3 radicals whereas the growth of (111) facets is accelerated by C_2H_2. As the ratio increases the (111) facets grow faster and therefore disappear first leaving the (100) facets exposed.[63] It was hoped that the uniform (100) nature of sample Si_13 could lead to more single crystal-like growth. The conditions used for sample Si_13 (10% CH_4 and 120 torr) were therefore chosen to be used for all remaining samples grown using MWPCVD. Interestingly, the standard conditions used previously for the MWPCVD reactor were 120 torr with 4 % CH_4 (although a total of 312.5 sccm) showing the standard conditions used are likely to produce high-quality diamonds (comparable to sample Si_10).

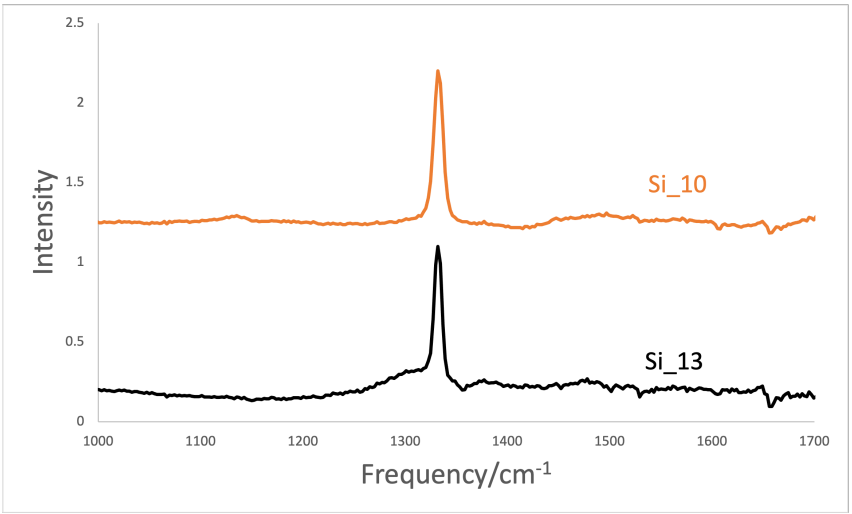

Figure 25: *Raman spectra of samples Si_10 (orange) and Si_13 (black) using 514 nm wavelength showing the diamond peaks at 1332 cm^{-1}.*

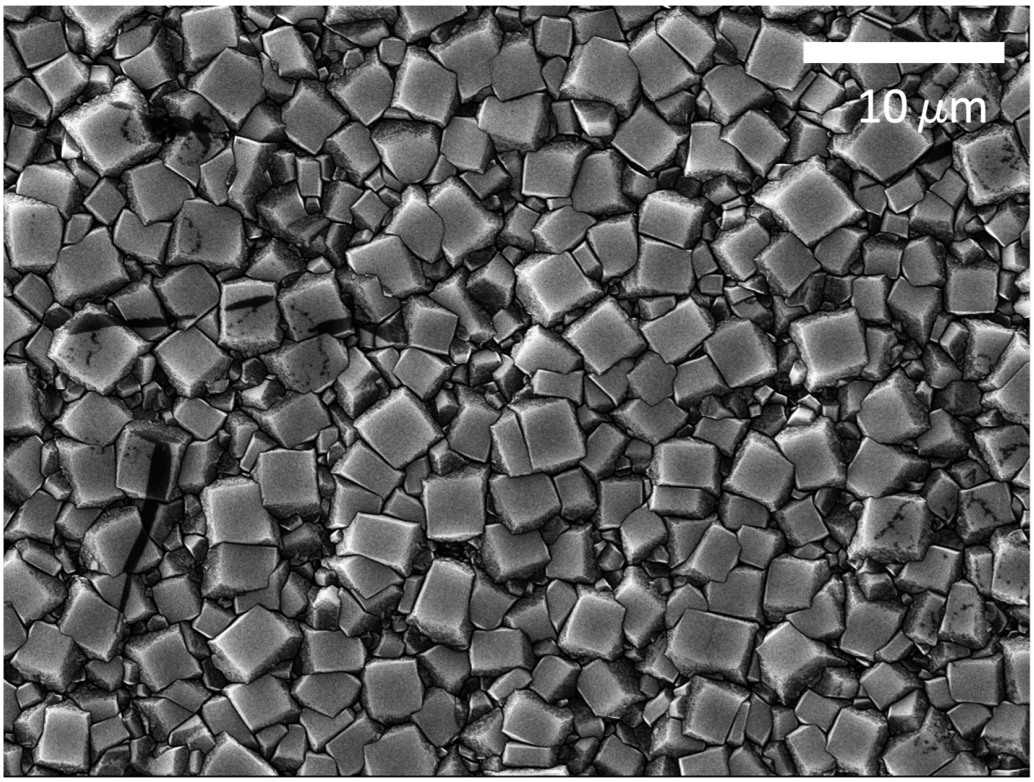

Figure 26: *SEM images of sample Si_13.*

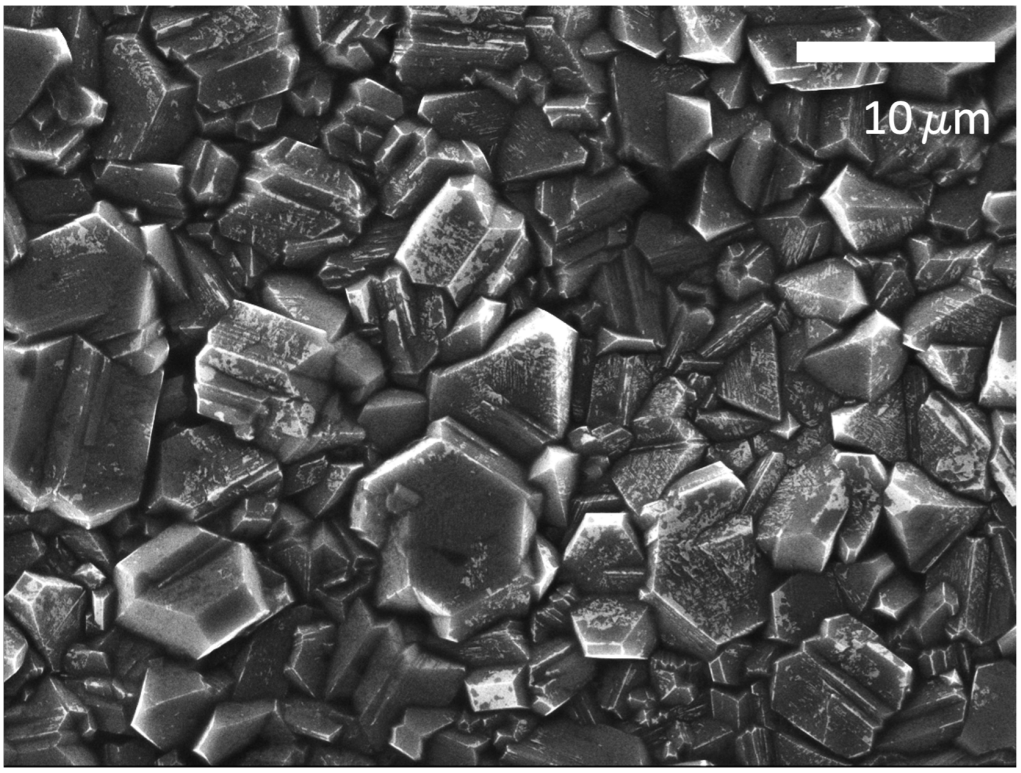

Figure 27: *SEM image of sample Si_10.*

One of the limitations of this data set however, was that only two variables, pressure and CH_4 percentage were altered. These were chosen as several previous papers (for example Linnik and Schreck) highlighted these as important variables, when attempting to grow SCD.[23,62] An important variable which could also be considered would be the input microwave power. All MWPCVD samples were grown using 1200 W (a 10:1 power to pressure ratio for the optimised conditions), however if the effect of changing the power had been investigated, it may have affected the optimal pressure for the system. It is unclear whether the 120 torr pressure contributed to the large, uniform crystals or if it was simply the power to pressure ratio that was optimal. Secondly, all data from this set was obtained with a constant total flow rate (600 sccm) so again, the conclusion that the conditions of 10% CH_4, 120 torr were the best, was limited to a total flow rate of 600 sccm.

Temperature during the CVD process is very hard to control therefore was not one of the parameters chosen to be investigated. Although the spacer wire can help to control the temperature, it cannot accurately and reliably determine specific, reproducible temperatures. All other factors that influence the plasma (power, pressure, flow rate, CH_4 concentration and more) affect the temperature so, as the results indicate, a precise consistent temperature was unachievable. Even if the temperature could have been accurately controlled, the single wavelength pyrometer that measured the temperature, produced readings which could only be used as a rough guide. Ideally, a two-colour pyrometer would have been used to determine the temperature of the substrate more accurately, however this was not possible as one of the commonly used wavelengths overlaps with the emission from the CVD plasma, interfering with the reading. Additionally, the display was calibrated for the substrate, not diamond which meant that once the film was thick enough the reading became unreliable, however it cannot be determined at exactly what time during the growth this happened. The combination of these difficulties and uncertainties meant that the temperature recorded for all MWPCVD growths, was only an estimate and could not be carefully controlled.

Finally, consideration must be given to the fact that the optimal conditions would have depended on the substrate. Si was chosen for the optimisation process due to the ease of growing diamond on Si over other substrates such as Mo, on which diamond has a tendency to delaminate (discussed in section 2.3). Although the conditions were ultimately to be used with Ir substrates, there was limited availability of Ir on YSZ and it was also extremely expensive, so the cheap, readily available Si substrates were used to initially test the parameters. However, despite growing relatively large, uniform crystals on Si this was not necessarily true for Ir or Mo substrates. Had more Ir substrates been available, it would have been better to use Ir rather than Si for the optimisation process, given the final goal was to grow large grains on Ir.

2.2 Growth on iridium

Before attempting to optimise the conditions for single crystal-like growth on Ir, it was necessary to determine if any diamond films could be successfully grown in the MWPCVD reactor, on unseeded Ir. The first sample (Ir_1a) did not show any successful growth. The conditions chosen were 1% CH_4 (6 sccm) at 50 torr and a 0.2 mm spiral was used as the spacer. It was likely that the conditions led to very low temperatures. However, due to the nature of the pyrometer and connected display, the emissivity value to calibrate the pyrometer could not be set low enough for Ir, so no temperature readings could be recorded for the Ir substrates. This made the growth of diamond on Ir even more challenging. On the assumption that the temperature under these conditions was too low, sample Ir_1b was run using the same conditions but with a 0.3 mm wire. Figure 30c shows there was some success, with high-quality diamond crystals appearing in some areas of the substrate, however it seemed likely that all nucleation had occurred on an apparent scratch on the surface. Despite that, this sample demonstrated that diamond could be grown on the Ir substrates in the MWPCVD reactor. The optimised conditions discussed above, in section 2.1, were then used for all subsequent MWPCVD Ir growths.

The second Ir sample (Ir_2) was grown in the HFCVD reactor to compare the results to the MWPCVD reactor. However, there was limited control of the variables in the HFCVD reactor, so growth conditions could not be optimised. The sample was run for four hours but no diamond growth was observed and a black layer of graphitic carbon was found on top of the Ir. Limited substrate availability meant it was decided not to investigate the growth on Ir using HFCVD any further.

Having identified 10% CH_4 (60 sccm) and 120 torr as the optimal conditions for the MWPCVD reactor, Ir_3 was grown for 21 hours using these conditions. The sample had visibly changed during the growth and Raman data confirmed the presence of some diamond crystals (figure 28). However, the Raman spectrum also indicated the presence of some sp^2 carbon (G and D peaks were present) and SEM images revealed very low-quality, ballas diamond. As described in a paper by Haubner and Lux, "non-optimal" conditions can lead to the formation of ball-like or cauliflower shaped polycrystalline ballas layers. This can be caused by too high a CH_4 concentration or too low a plasma intensity but the exact point at which these ballas layers begin to form is very dependent on the specific system in use. Temperature also has an important influence over the appearance of the diamond films. Although the direct effect of temperature is difficult to analyse directly, because it is influenced by so many factors, Haubner and Lux offered a possible explanation as to why higher temperatures (above about 1000°C) can lead to ballas diamond growth. As temperature increases, the hydrogen on the hydrogen terminated surface begins to desorb at a much faster rate, leaving the surface prone to reconstruction and the formation of defects. At the higher CH_4 concentrations, there are insufficient H radicals to etch away the defects,

leading to poor quality diamond or even graphite. Interestingly, the progression from ballas through (100) facets to well-faceted diamond outlined by Haubner and Lux shown in figure 29, matched well to the SEM images of samples Ir_1b, Ir_3 and Ir_4 (figure 30).[64] Another possible explanation for the ballas diamond growth is that only a very small number of nucleation sites were formed (as Ir self-nucleates at the start of the CVD process so was not pre-seeded), meaning each nucleus could expand and grow rapidly outwards as well as upwards, leading to ball-shaped growth.

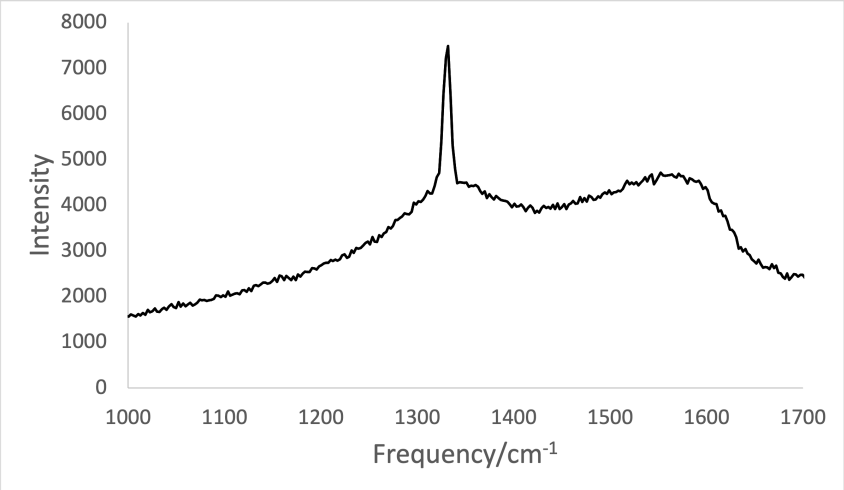

Figure 28: *Raman spectrum of sample Ir_3 using 514 nm wavelength. Shows the diamond peak at 1332 cm^{-1} along with both the D and G sp^2 peaks.*

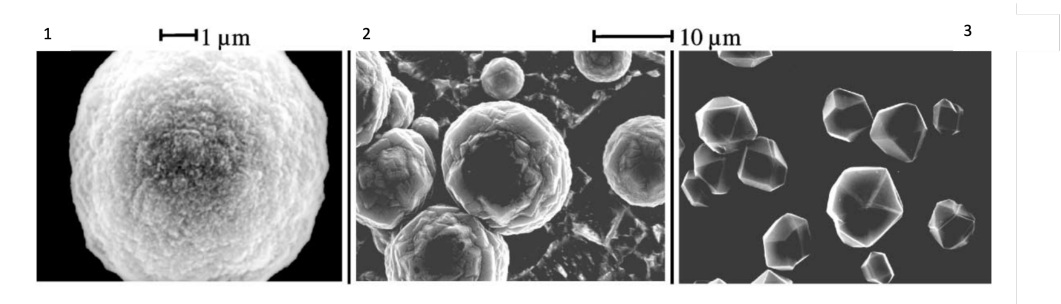

Figure 29: *Image showing progression from 1. ballas, 2. (100) facets on complex structure, 3. well-faceted diamond. From Haubner and Lux.*[64]

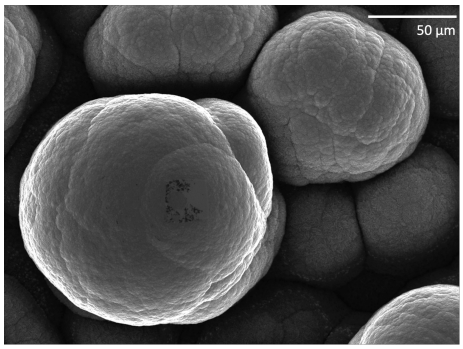

(a)

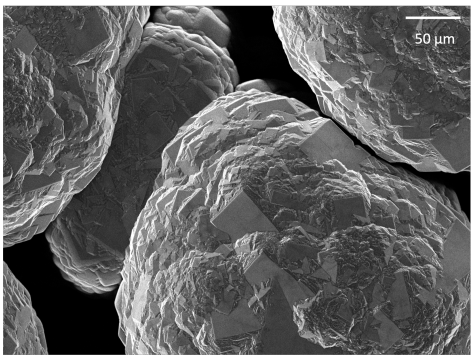

(b)

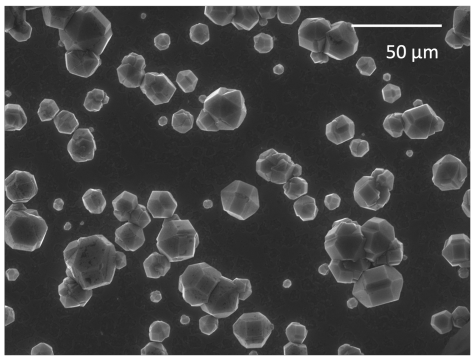

(c)

Figure 30: *a) Sample Ir_3 showing the ballas layer, b) sample Ir_4 showing (100) facets on the still ballas-like structure, c) sample Ir_1b showing well-faceted diamond crystals.*

The dramatic change in appearance between sample Ir_1b (figure 30c) and samples Ir_3 (figure 30a) and Ir_4 (figure 30b) can be attributed to the significant change in conditions. The CH_4 concentration had been increased by a factor of 10 (6 sccm to 60 sccm), which is the most likely cause of the observed ballas growth. However, the pressure was increased, from 50 torr to 120 torr, and therefore plasma intensity had also increased which could have been a factor that favoured the ballas layers seen in figure 30a. Although it is difficult to directly compare temperatures between the two sets of conditions used, the higher pressure and presence of ballas-like growth suggests both samples Ir_3 and Ir_4 experienced higher substrate temperatures than sample Ir_1b. It is unknown what the diamond quality would have been if sample Ir_1b had also been run for 21 hours, so the elapsed time of the runs may also play an important factor, however the ballas diamond was present all the way through when the cross section of Ir_4 was examined.

The differences between samples Ir_3 and Ir_4 were slightly more subtle. Both samples were run at 120 torr and 60 sccm CH_4 (10%) but the spacer wires used were different (for Ir_3 a 0.25 mm wire was used whereas for Ir_4 a 0.15 mm wire was used). This indicated that the major factor affecting the different appearance of the films was temperature. Ir_4 would have been at a lower temperature throughout and resulted in fewer ballas-type structures and

more (100) facets. This result supported the theory outlined above that ballas diamond is more likely to grow at higher temperatures. It is worth noting that samples Ir_3 and Ir_4 were very fragile and sample Ir_4 actually split during growth. This may have been due to the extremely large ballas structures within the crystals but indicated that, as well as the very poor quality diamond, these samples would not have been suitable for detection devices.

Finally, another factor to consider when discussing diamond growth on Ir is nucleation. BEN conditions lead to high-quality nucleation however are unsuitable for diamond growth. It is therefore likely that in the MWPCVD reactor the optimal conditions for nucleation and growth on Ir are not the same. This may be another reason for the low-quality ballas diamond produced and had the conditions used for the initial nucleation stage been different to those used for the majority of the growth, higher quality diamond may have been achieved.

2.3 Devices

Due to the disappointing results from the Ir runs, it was decided to make the first devices using polycrystalline diamond films, grown on Mo substrates. Despite being harder to grow diamond on Mo, due to its large thermal expansion often causing samples to delaminate, it was chosen over Si, because in order to apply a potential difference across the devices, an ohmic contact was required. Figure 31 shows an SEM image of the surface of the diamond grown on Mo, which illustrates that, although better than the diamond grown on Ir, the uniformity was not as good as sample Si_13 and the large number of grain boundaries may have caused issues when being used as a detector. The average grain size for this sample was 2.95 μm, approximately half that of the Si sample using the same conditions.

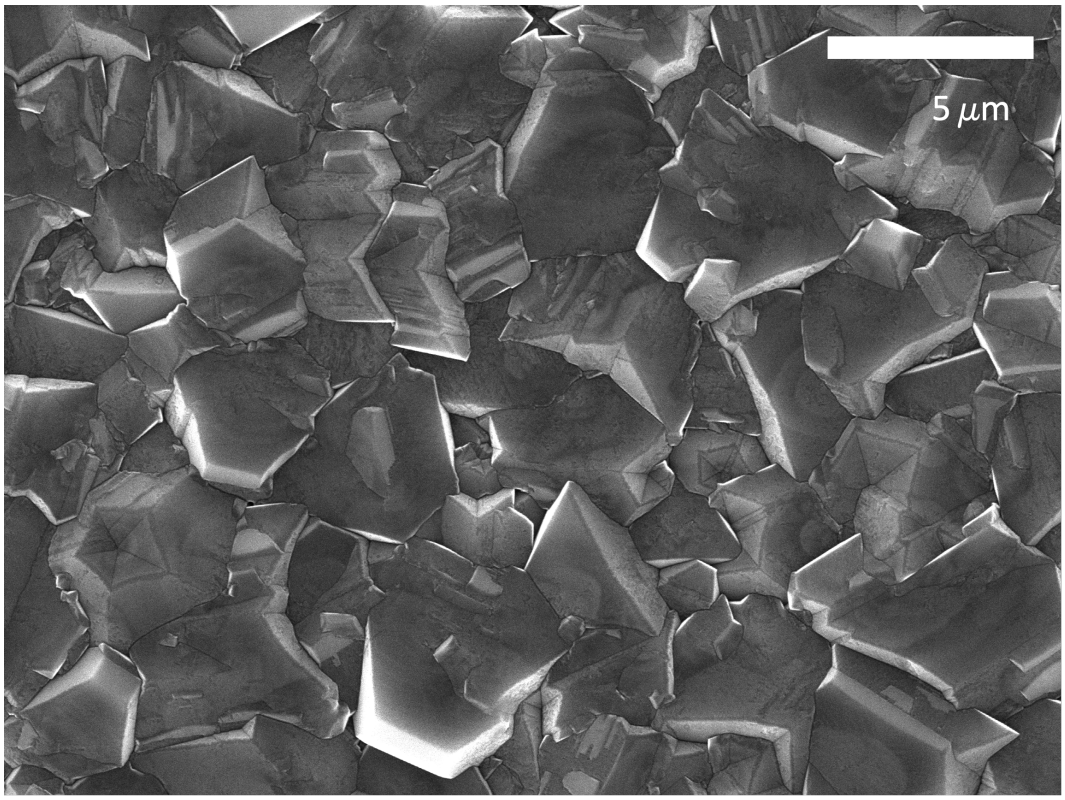

Figure 31: *SEM image of the diamond on Mo used in the first devices.*

The results from the Ir and Mo samples highlight the influence that the substrate can have, as well as the conditions; identical conditions can lead to very different diamond growth on different substrates. However, it is difficult to distinguish between the effects of the initial substrate and the seeding. The Si samples were seeded using electrospray seeding, a very uniform technique, the Ir self-nucleates and the Mo samples were seeded using manual abrasion. Self-nucleation could have resulted in fewer nuclei being present, in turn leading to ballas diamond and manual abrasion is not as uniform as electrospray seeding which could explain why the diamond films did not show the same uniform grains. Overall though, both the seeding and the substrate affect the diamond quality and therefore, ideally, conditions would be optimised for each substrate individually.

Despite the diamond being less than ideal quality, a number of devices were fabricated using diamond on Mo, in order to produce some prototypes of various designs. Three different designs, using Mo substrates, were assembled and are shown in figure 32. Both MIM and PIM designs were fabricated in order to compare both structures. As explained in section 1.5.1, the beta particles from the decay of tritium are very low energy and therefore, a very thin top contact was required for the devices, in order to allow the beta particles to penetrate through to the diamond layers. Unfortunately, the polycrystalline nature of the Mo devices meant that the surface was uneven and therefore the top contacts had to be thicker than if the

samples had been a smooth layer of SCD. An amorphous, conducting layer of carbon with Al at the corners was chosen as well as just Al, in order to allow for comparison. The way the devices were designed meant that only the centre of the device would be exposed to the radiation.

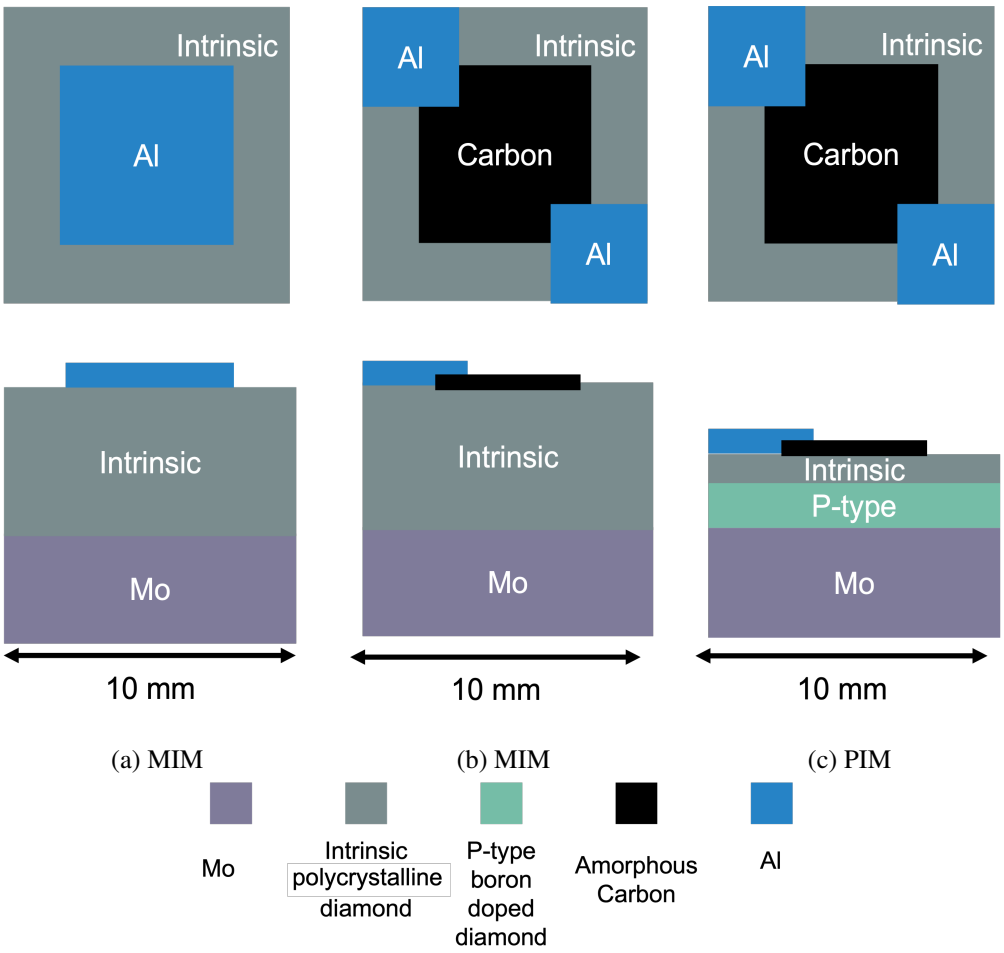

Figure 32: *Schematic of structure of three Mo device designs. Upper row images show top-down view and lower row images show a cross sectional view, a) MIM device with 10 µm layer of intrinsic diamond with Al top contact, b) MIM device with 10 µm layer of intrinsic diamond with amorphous carbon top contact and Al corner contacts, c) PIM device with 3 µm layer of BDD and 2 µm layer of intrinsic diamond with amorphous carbon top contact and Al corner contacts.*

A second set of devices, made from SCD samples (5 x 5 mm, 0.3 mm thick) supplied by Appsilon Enterprise, were also fabricated. Two slightly different designs were made (figure 33), one with Al contacts on the top (a direct comparison with the Mo devices), and the other with a layer of graphene on the top. Graphene was chosen as a top contact as it is only one atom thick therefore the low energy beta radiation, formed during the decay of tritium, can

easily pass through to the diamond film and be detected. The SCD was expected to have a much smoother surface than the Mo devices and therefore, it was hoped that graphene could act as a top contact. However, low energy electron diffraction (LEED) measurements of p-type Si wafer samples, which had undergone the same graphene transfer process, showed no diffraction pattern, indicating that either the graphene transfer process had been unsuccessful, or that the graphene had become damaged during the transfer process and contained no long range order. Both of these outcomes indicated that the graphene was not suitable to act as a top contact for the devices and it was likely that the graphene transfer onto the SCD substrates was also unsuccessful. The SCD substrates could not be tested directly as LEED required a conducting surface below the surface being imaged. These results demonstrated that more work was required to perfect the graphene transfer step.

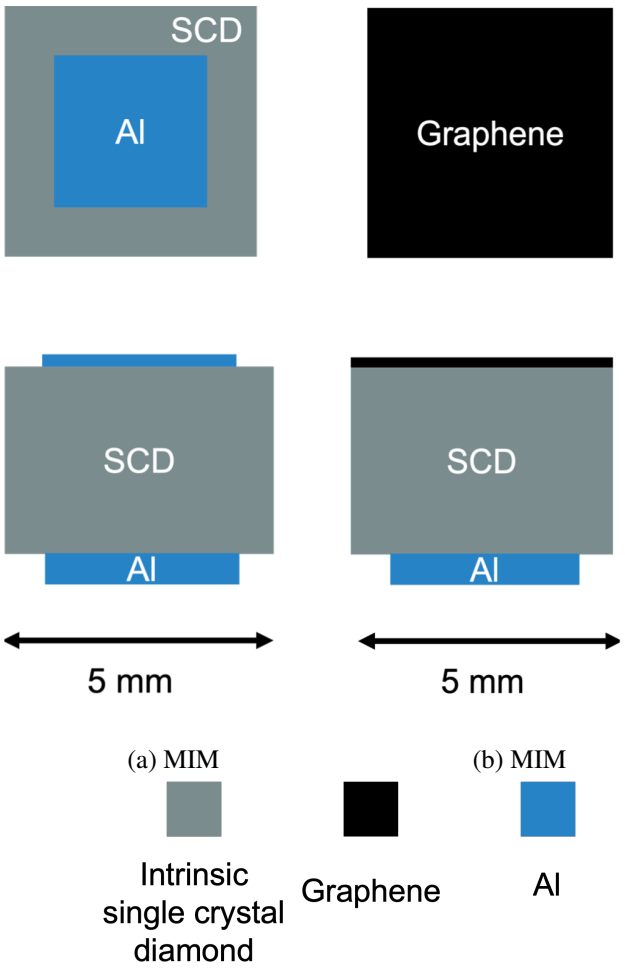

Figure 33: *Schematic of structure of the two SCD device designs. Upper row images show top-down view and lower row images show a cross sectional view, a) MIM device with 0.3 mm intrinsic SCD with Al top and bottom contacts, b) MIM device with 0.3 mm intrinsic SCD with Al bottom contact and graphene top contact.*

These devices were just the first designs in what will hopefully be many iterations of potential tritium detectors. In order to characterise and assess the potential of these devices to be used as detectors, both check source and electron beam (e-beam) tests would be carried out. Check source tests would involve a beta source being used above the devices, which would have a potential difference applied across them. An oscilloscope would be connected to the device and any current produced due to the radiation would be detected. E-beam tests would be carried out in an electron microscope, using the electron beam at various potentials, to fire at the device and probes would detect any current generated. Although this would not generate the small pulses seen in radioactive decay, the large range in potentials that could be applied (synonymous with activity), would allow for the testing of the sensitivity of the devices. Both of these tests would be looking to detect small changes in current, caused by the incident electrons, across the devices. In order for the devices to detect any changes in current, the current leakage (background current or noise), when a potential difference was applied across the device, with no beta source present, would need to be very small (of the order of 10s of pA). Initial tests, to measure the current leakage, indicated that the polycrystalline diamond-on-Mo devices measured a much larger current than would be required (of the order of a few hundred μA). However, as expected, the SCD devices measured much more promising currents (around 0.01 pA), that were six orders of magnitude lower than the Mo devices. The initial results indicate that these first Mo devices may be unable to detect any small increases in current caused by radiation but the SCD devices could be more promising. The low current leakage and therefore very high resistance of the SCD, is what makes diamond such a good radiation detector. Overall these results appear to fit with what was expected; SCD is the ideal substrate for a diamond tritium detector.

3 Conclusions

Optimisation of the MWPCVD reactor for seeded Si samples led to the conclusion that within the parameters investigated, 120 torr and 10% CH_4 produced the largest and most uniform diamond grains. This was limited to a power of 1200 W and a total flow rate of 600 sccm and was assessed based on SEM images, average grain size and the thickness of the films. The grains produced by using the 120 torr and 10% CH_4 conditions, run for three hours, had an average grain size of approximately 6 μm and formed very uniform (100) crystals. When these conditions were used with Ir, the result was very low-quality ballas diamond. This was thought to be caused by several factors, including a high CH_4 concentration and high temperatures. Mo substrates were then used to fabricate a first set of detection devices, however the diamond quality was not quite as good as Si, with an average grain size of about 3 μm (half that of Si). It was therefore concluded that, along with conditions such as pressure and CH_4 concentration, the substrates used and the seeding technique also had a huge influence on diamond quality.

Using the results from the optimisation of the conditions for the MWPCVD, several device designs were fabricated using polycrystalline diamond on Mo. Both MIM and PIM designs were fabricated and both carbon and Al were used as top contacts. Alongside the devices using the polycrystalline diamond, some SCD substrates were obtained and used to fabricate a second set of devices. Although not completed yet, check source and e-beam testing will be done to compare the designs. Initial current leakage measurements indicate, as expected, that the SCD devices are more sensitive, and show more potential, than the polycrystalline Mo devices, for use as tritium detectors.

4 Future Work

4.1 Optimisation of MWPCVD conditions

4.1.1 Silicon

In this study the pressure and CH_4 concentrations were varied, however many other parameters also affect the quality of CVD diamond films. For example, an interesting set of experiments could be carried out by varying the applied power and pressure whilst retaining a constant ratio of power to pressure. This would affect the size and intensity of the plasma so would therefore also influence the diamond films. A second parameter that could easily be investigated would be the total flow rate, which could be varied whilst keeping the proportions of gases constant. At constant pressures, the higher the flow rate the less time the individual gas molecules, and associated radicals, spend in the chamber and therefore the less time they have to react. This is likely to change the composition of the mixture of gases and radicals near the surface of the substrate, so therefore would also affect the diamond growth.

Although temperature is hard to control, it is also a key factor which determines the quality of the diamond, as discussed in section 2.2. If all other parameters (power, pressure, flow rate, gas composition) were kept constant, by changing the spacer wire to alter the temperature this could be investigated. The lack of precision associated with the pyrometer would mean accurate readings could not be taken, however any trends seen by increasing the temperature would be reliable. It is likely that very little growth would be observed below 600° C however as the substrate begins to reach temperatures significantly higher than about 1000° C it is likely that more and more graphite would be observed.[19]

4.1.2 Iridium

Optimisation of the MWPCVD reactor conditions for growth on Ir substrates has not been fully explored. Ideally, a large number of Ir substrates would be required in order to do a similar set of experiments to the 12 Si runs detailed in this report. Initially, just pressure and CH_4 concentration could be varied, but further studies similar to those discussed above for Si could then be carried out. Based on samples Ir_3 and Ir_4, a thinner spacer wire than was used for equivalent Si runs should be used in order to reduce the temperature of the Ir substrate and prevent the growth of ballas diamond. A pyrometer, that can be correctly calibrated for Ir substrates, would also be required to establish the temperature at which the diamond films were growing.

One of the main differences when using Ir compared to Si is that Ir is self-nucleating, so is not initially seeded. Given that the low pressure, low CH_4 concentrations appeared to give some high-quality nucleation (although this may have been due to a scratch providing

suitable nucleation sites), runs where the initial conditions are low CH_4, low pressure to induce nucleation, followed by an increase in CH_4 and pressure, may result in interesting, and potentially higher quality films. Alternatively, starting with a higher CH_4 concentration may help to increase nucleation followed by a lower CH_4 concentration used for the majority of the run, similar to the methods described by both Yugo and Schreck.[25,65] Again, several runs would have to be compared in order to optimise the conditions, and to maximise the number of nucleation sites, which could help to reduce the ballas diamond growth.

4.2 Devices

4.2.1 Boron doping

Although BDD was used in the PIM devices, it would have been useful to know the boron concentration within the diamond. Sufficient boron was required to produce a p-type semiconductor, however too much boron could have resulted in the diamond exhibiting more metallic-like properties, for example conductivity decreases with temperature.[66] Before producing the PIM devices, several BDD films were grown on Si, in order to investigate the boron concentration, using secondary ion mass spectrometry (SIMS) to determine the composition of the films. Unfortunately, this technique was unavailable for the duration of the project. Comparisons between samples run with 0.02% B_2H_6 and samples done using the residual doping within the chamber, might have provided accurate measurements of boron concentrations, which would have helped to improve the devices. Mortet *et al.* showed that Raman data could be used to determine the boron concentration, by obtaining a standard BDD sample, with a known boron concentration.[34] However, this would not be as accurate as SIMS. Both SIMS and Raman could be used in conjunction with each other to create a calibrate for the boron concentration, leading to a more detailed characterisation, and therefore an improvement, of the devices.

4.2.2 Graphene contacts

Ideally more time would have been devoted to the evaluation of the graphene transfer step and improvements made. A reliable characterisation technique would be useful to determine if each step in the transfer process had been successful. LEED was used to determine if the transfer had been successful but this is an expensive and time consuming technique. A technique that can be performed quickly, and in the same place as the graphene transfer process, would be favoured. Raman was unsuccessful in detecting the graphene at any stage (including initially on the copper), however an effort to reduce the fluorescence could help to make Raman a useful tool. Additionally, Kim *et al.* showed that interference effects observed through an optical microscope could also be used to identify any graphene on the surface, which would be worthy of investigation in the future.[67]

4.2.3 Device testing and improvement

As detailed in section 2.3, check source and e-beam testing on the first iteration of devices would enable comparisons of the structure and design of the devices. Following on from this, improvements to the quality of the devices could be made by adjusting variables such as the thickness, boron doping (PIM devices), and top and bottom contacts. Ideally, several iterations of the device designs would be fabricated, leading to an improvement in the effectiveness and sensitivity of the devices, eventually leading to the use of diamonds as tritium detectors in fusion reactors.

4.2.4 Single crystal diamond

Ultimately, in order to produce the most effective devices, the long-term goal would be to grow SCD. Ideally, BEN would be used with Ir substrates and a range of conditions would need to be optimised and evaluated in the MWPCVD reactor, as discussed in section 4.1.2. Alternatively, new techniques to grow SCD could be established using equipment already available, which would help to improve the effectiveness and sensitivity of the devices.

5 Experimental details

5.1 Diamond growth

5.1.1 Substrates

All substrates used during diamond growth were 10 mm x 10 mm samples. The Si was cut from a single wafer using an Oxford Lasers laser cutting and machining system and was intrinsic, non-conducting Si. The Ir substrates, prepared *via* magentron sputtering by Rebecca Nichols of the University of Bristol Physics department, were 100 nm single crystal Ir (111) samples grown on YSZ (111). The Mo substrates were purchased backed with masking tape and cut using a water jet.

5.1.2 Seeding

Different seeding techniques were used depending on the substrate in question. For the Si samples, electrospray seeding was chosen for thin, uniform coverage. Figure 34 shows the equipment, up to six samples could be stuck to the metal spinning plate within the box. The samples were cleaned with methanol before use. A pre-made solution containing ten drops of detonation nanodiamond colloid solution (2% w/v in water, NanoAmando Colloid 3.3 $\pm$ 0.6 nm) in 30 ml methanol was used to fill a syringe and a potential difference of 32.5 kV was applied across the tip. When the solution had been left for longer than a few days it was sonicated for an hour before use. The samples were left for $\sim$ 30 minutes until all the solution had been used up and then the syringe was refilled with methanol to wash the system through.

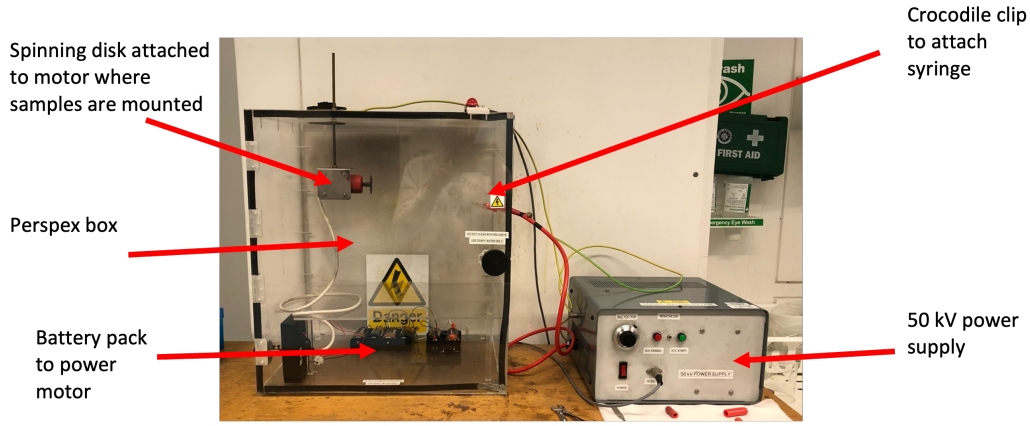

Figure 34: *Equipment used for electrospray seeding.*

The other seeding technique used for the Mo samples was manual abrasion. Diamond does not adhere as effectively to Mo as it does to Si, so this technique was chosen as it helps to embed the diamond into the Mo surface, helping the diamond film to remain attached to the Mo substrate. The Mo substrates were cleaned with methanol before a very small

amount of microdiamond (Van Moppes, PM2, 2.0 ± 1.0 μm) was placed between two of the substrates and rubbed together for about 5 minutes. The nanodiamond was then washed off with methanol, leaving the surface of the Mo substrates rough with lots of defects, that could act as nucleation sites.

5.1.3 MWPCVD

For all microwave runs a 1.5 kW, 2.45 GHz MWPCVD ASTeX type reactor was used which was run at a power of 1200 W. The gas flow rates, measured in standard cubic centimetres per minute (sccm), were controlled by mass flow controllers (MFCs) and the pressure was controlled by an automatic pressure gauge. Figure 35 shows the reactor used and associated components. The samples were mounted on a tungsten disk on the platform with a spacer wire between the metal plate and disk. The spacer wire creates a gap between the baseplate and disk and adjusting the height of the gap, adjusts the thermal contact between them, and therefore provided some control over temperature. The plasma was struck at 45% power (675 W) under a 15 torr H_2 atmosphere, after which the pressure and power were slowly increased, and the CH_4 was added at $\sim$ 50 torr. The timer was started once the power reached 1200 W. At the end of the runs the CH_4 was turned off and the sample was left in a H_2 plasma for 2 minutes before the pressure and power were slowly wound down simultaneously.

Temperature readings were taken from a digital display connected to a single wavelength (2.2 μm) pyrometer. The pyrometer measured the absorbance at 2.2 μm, and provided the emissivity value was calibrated correctly, could give an estimate of the temperature. The emissivity value used to calibrate the pyrometer for Si was 0.19, and for Mo was 0.17. The emissivity value for Ir was out of range so no temperature measurements could be taken for Ir samples.

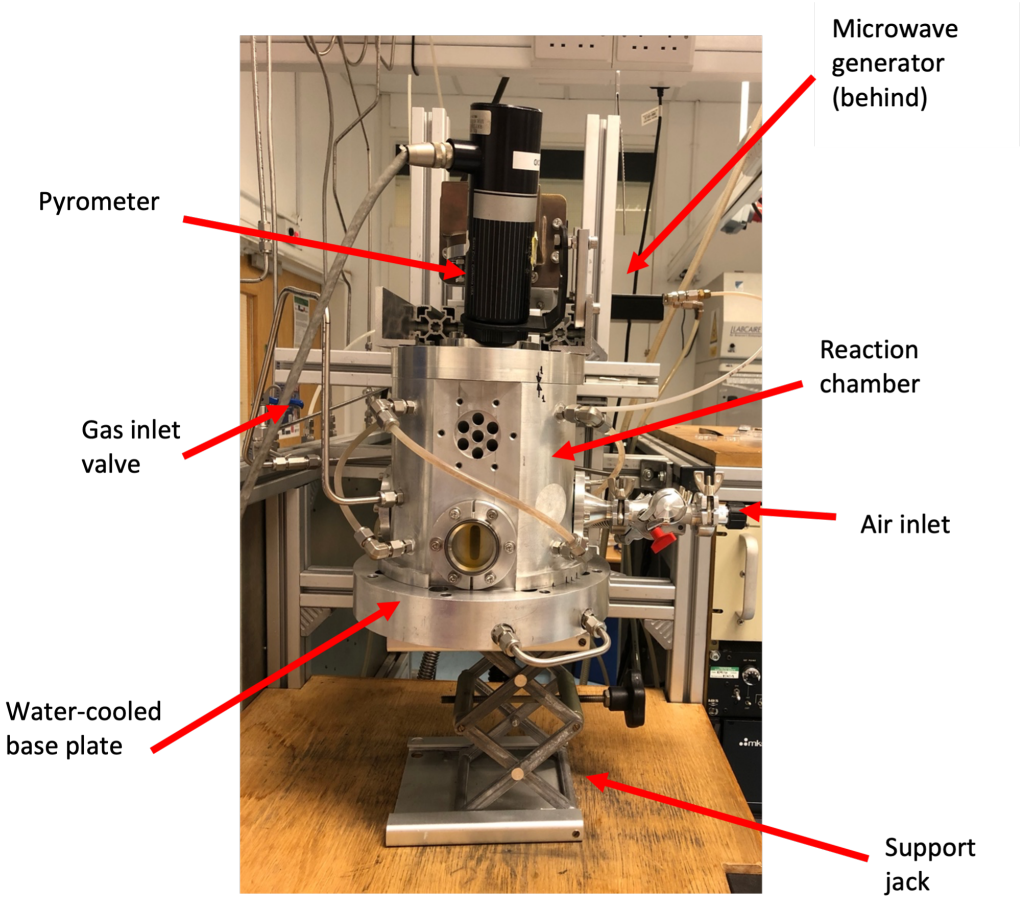

Figure 35: *MWPCVD reactor used to grow samples.*

5.1.4 HFCVD

HFCVD samples were made using HFCVD reactors assembled in the Bristol Diamond Laboratory (figure 36), consisting of a 2-stage rotary pump, 25 A mains power supply and a nichrome heater to ensure good substrate temperature. The reactor was loaded with three tantalum filaments (7 cm long, 0.25 mm thick, 0.5 cm spacing) and up to three substrates and was left to pump down overnight. The working conditions were 20 torr with the following flow rates: 200 sccm for H_2, 2.0 sccm for CH_4 and 0.7 sccm for B_2H_6 (5% B_2H_6 in H_2). The heater was run at a current of 4.0 A and a current of 25.0 A was passed through the filaments. The filaments were changed after five hours for all the 10 hour growth runs. Any runs done with residual boron doping were run under the same conditions except the B_2H_6 was not flowed.

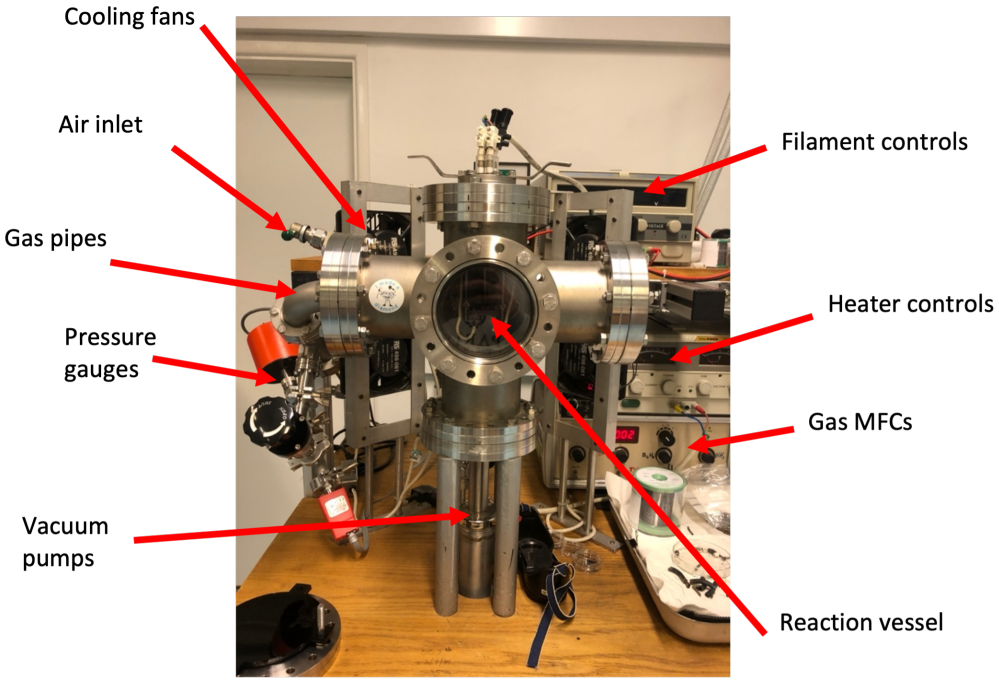

Figure 36: *HFCVD reactor used to grow the BDD samples.*

5.2 Device preparation

5.2.1 Carbon layer

A Quorum Q150TES turbo-pumped sputter coater was used to deposit the amorphous carbon layers, using graphite rods. The samples were masked using masking tape around the edges so that only the centre was covered and a 10 nm layer was deposited.

5.2.2 Aluminium contacts

An Edwards Evaporator (figure 37) was used to deposit Al contacts onto the corners and centres of various substrates. Al wire was wrapped around the tungsten filaments and heated under vacuum until the desired thickness of Al had been reached. An oscillating quartz gauge was used to measure the thickness of Al deposited. The base pressure was 5.8 x 10^{-6} Pa before deposition was started. Samples were masked using parafilm to achieve the desired contacts.

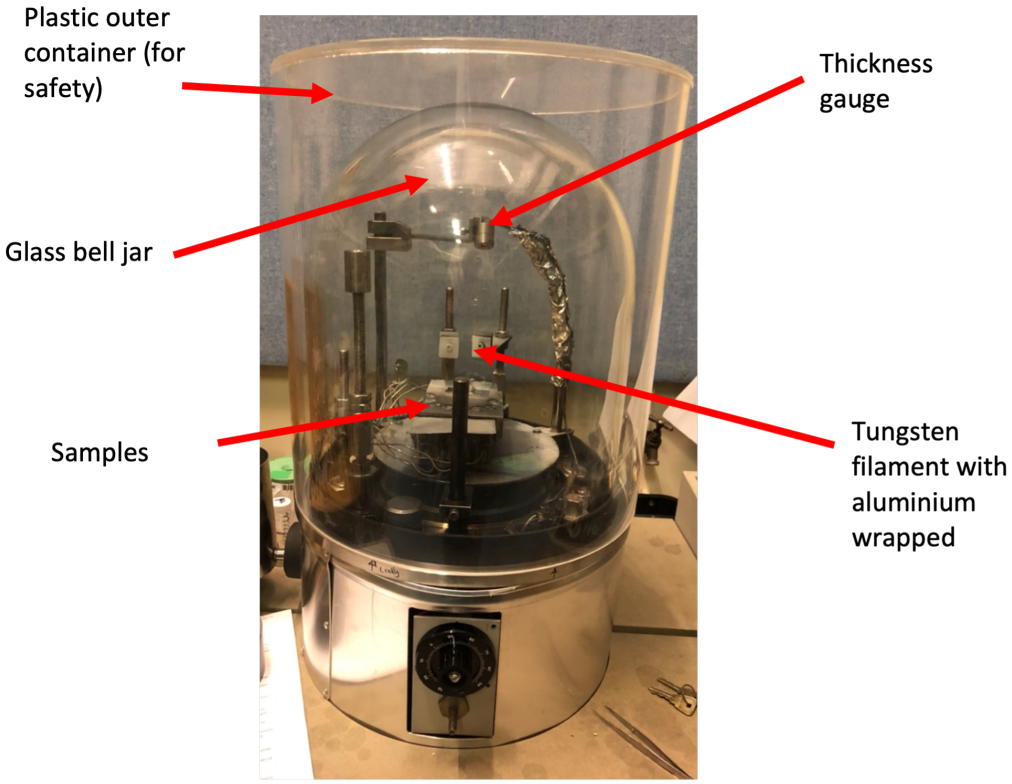

Figure 37: *Edwards Evaporator used to add Al contacts.*

5.2.3 Graphene

The graphene transfer method was adapted from Shivayogimath *et al.* and a monolayer 150 x 150 mm of graphene on copper was obtained from Grolltex .[68] Films of polyvinyl acetate (PVA) were made by painting PVA glue onto strips of non-stick paper and left to dry overnight. Three or four layers of PVA glue were applied in order to obtain a substantial film. A laminator was then used to transfer the graphene from the copper onto the PVA films, the copper was placed on top of the paper backed PVA films which were then placed in a non-stick paper packet (figure 38a). The samples were put through the laminator 10 times before being left on a hot plate at 110 °C for five minutes with a weight on top (figure 38b). This processes of lamination followed by the hot plate was then repeated transferring the graphene from the PVA film to the substrate. Finally, the samples were left in deionised, room temperature water overnight to allow the PVA to dissolve.

(a) (b)

Figure 38: *Images of the graphene transfer process, a) shows the graphene on copper placed on the paper backed PVA film within the non-stick paper packet, b) shows the sample after being laminated on the hot plate.*

5.3 Characterisation

5.3.1 Raman

Raman measurements were carried out using a Renishaw 2000 laser Raman spectrometer with a 514 nm green laser. The magnification of the lens used to focus the microscope was x50 and the laser power was adjusted based on the sample. All spectra were acquired using cosmic ray removal, with 10, six-second-long acquisitions, and the central wavenumber set to 1332 cm^{-1}. The spectra included in the main sections of this report were normalised and the fluorescence removed.

5.3.2 SEM

SEM images were taken in the University of Bristol Chemistry department imaging facility using a Jeol IT300 SEM instrument. An Oxford Lasers laser cutting and machining system was used to cut any samples in half in order to image the cross sections. These samples were mounted at a 70° angle so the measurements of thicknesses had to be adjusted accordingly. During SEM, a beam of electrons is fired towards a surface which can be scattered or cause the emission of a second set of electrons from the surface. All these electrons are then detected and an image of the surface topology can be formed.[69]

5.3.3 LEED

Low energy electron diffraction (LEED) was carried out using the nanoESCA facility in order to attempt to image the graphene on the surafces. The graphene was transferred onto conducting p-type Si and LEED was carried out using an electron energy of 500 eV.

6 Bibliography

References

[1] M. N. R. Ashfold, P. W. May, C. A. Rego and N. M. Everitt, *Chem. Soc. Rev.*, 1994, **23**, 21–30.

[2] M. Weller, J. Rourke, T. Overton and F. Armstrong, in *Inorganic Chemistry*, Oxford University Press, 7th edn., 2018, ch. 14, p. 413.

[3] Structures of allotropes of carbon, https://www.chemtube3d.com/claydencarbonallotropes/, (Accessed 08/02/22).

[4] J. Ristein, *Surface Science*, 2006, **600**, 3677–3689.

[5] R. Robertson, J. J. Fox and A. E. Martin, *Philosophical Transactions of the Royal Society of London. Series A, Containing Papers of a Mathematical or Physical Character*, 1933, **232**, 463–535.

[6] G. Sutherland, D. Blackwell and W. Simeral, *Nature*, 1954, **174**, 901–904.

[7] C. M. Breeding and J. E. Shigley, *Gems & Gemology*, 2009, **45**, 96–111.

[8] P. W. May, *Philosophical Transactions of the Royal Society of London. Series A: Mathematical, Physical and Engineering Sciences*, 2000, **358**, 473–495.

[9] W. G. Eversole, US Patents 3030187, 3030188, 1958.

[10] J. C. Angus, A. Argoitia, R. Gat, Z. Li, M. Sunkara, L. Wang and Y. Wang, *Philosophical Transactions: Physical Sciences and Engineering*, 1993, **342**, 195–208.

[11] B. Derjaguin, D. Fedoseev, V. Lukyanovich, B. Spitzin, V. Ryabov and A. Lavrentyev, *Journal of Crystal Growth*, 1968, **2**, 380–384.

[12] D. J. Poferl, N. C. Gardner and J. C. Angus, *Journal of Applied Physics*, 1973, **44**, 1428–1434.

[13] B. Spitsyn, L. Bouilov and B. Derjaguin, *Journal of Crystal Growth*, 1981, **52**, 219–226.

[14] V. V. S. S. Srikanth, P. S. Kumar and V. B. Kumar, *International Journal of Electrochemistry*, 2012, **2012**, doi:10.1155/2012/218393.

[15] S. Ohmagari, K. Srimongkon, V. Amornkitbamrung, H. Yamada, A. Chayahara and S. ichi Shikata, *Transactions of the Materials Research Society of Japan*, 2015, **40**, 47–50.

[16] S. Matsumoto, Y. Sato, M. Tsutsumi and N. Setaka, *Journal of Material Science*, 1982, **17**, 3106–3112.

[17] M. Roy, in *Materials Under Extreme Conditions*, ed. A. Tyagi and S. Banerjee, Elsevier, Amsterdam, 2017, ch. 8, pp. 259–292.

[18] M. Kamo, Y. Sato, S. Matsumoto and N. Setaka, *Journal of Crystal Growth*, 1983, **62**, 642–644.

[19] R. Haubner, *ChemTexts*, 2021, **7**, 10.

[20] P. K. Bachmann, D. Leers and H. Lydtin, *Diamond and Related Materials*, 1991, **1**, 1–12.

[21] K. Ohtsuka, K. Suzuki, A. Sawabe and T. Inuzuka, *Japanese Journal of Applied Physics*, 1996, **35**, L1072–L1074.

[22] M. J. Verstraete and J.-C. Charlier, *Applied Physics Letters*, 2005, **86**, 191917.

[23] M. Schreck, S. Gsell, R. Brescia and M. Fischer, *Scientific Reports*, 2017, **7**, 44462.

[24] M. Schreck, in *Comprehensive Hard Materials*, ed. V. K. Sarin, Elsevier, Oxford, 2014, vol. 3, pp. 269–304.

[25] S. Yugo, T. Kanai, T. Kimura, and T. Muto, *Applied Physics Letters*, 1991, **58**, 1036–1038.

[26] Y. Wang, W. hua Wang, S. lin Yang, G. yang Shu, B. Dai and J. qi Zhu, *New Carbon Materials*, 2021, **36**, 512–526.

[27] D. Li, M. H. Nielsen, J. R. I. Lee, C. Frandsen, J. F. Banfield and J. J. D. Yoreo, *Science*, 2012, **336**, 1014–1018.

[28] L. M. Sanzenbacher, PhD thesis, The Ohio State University, 2011.

[29] M. Weller, J. Rourke, T. Overton and F. Armstrong, in *Inorganic Chemistry*, Oxford University Press, 7th edn., 2018, ch. 14, pp. 138–143.

[30] P.-A. Glans, T. Learmonth, K. E. Smith, S. Ferro, A. De Battisti, M. Mattesini, R. Ahuja and J.-H. Guo, *Applied Physics Letters*, 2013, **102**, 162103.

[31] R. Kalish, *Carbon*, 1999, **37**, 781–785.

[32] S. Conejeros, M. Z. Othman, A. Croot, J. N. Hart, K. M. O'Donnell, P. W. May and N. L. Allan, *Carbon*, 2021, **171**, 857–868.

[33] K. Su, Z. Ren, J. Zhang, L. Liu, J. Zhang, Y. Zhang, Q. He, C. Zhang, X. Ouyang and Y. Hao, *Applied Physics Letters*, 2020, **116**, 092104.

[34] V. Mortet, Z. V. Živcová, A. Taylor, M. Davydová, O. Frank, P. Hubík, J. Lorincik and M. Aleshin, *Diamond and Related Materials*, 2019, **93**, 54–58.

[35] D. Kania, M. Landstrass, M. Plano, L. Pan and S. Han, *Diamond and Related Materials*, 1993, **2**, 1012–1019.

[36] D. Jain, J. Nuwad, N. Manoj and V. Sudarsan, in *Materials Under Extreme Conditions*, ed. A. Tyagi and S. Banerjee, Elsevier, Amsterdam, 2017, pp. 683–715.

[37] R. Hofstadter, *Nucleonics*, 1949, **4**, 2–27.

[38] R. Hofstadter, *Proceedings of the IRE*, 1950, **38**, 726–740.

[39] H. Friedman, L. S. Birks and H. P. Gauvin, *Phys. Rev.*, 1948, **73**, 186–187.

[40] C. Raman and G. Rendall, *Proceedings of the Indian Academy of Sciences-Section A*, 1944, **19**, 265.

[41] G. Freeman and H. Van Der Velden, *Physica*, 1952, **18**, 9–19.

[42] K. G. McKay, *Physical Review*, 1950, **77**, 816.

[43] F. C. Champion and S. B. Wright, *Proceedings of the Physical Society*, 1959, **73**, 385–392.

[44] P. J. Kennedy and J. T. Randall, *Proceedings of the Royal Society of London. Series A. Mathematical and Physical Sciences*, 1959, **253**, 37–51.

[45] P. Dean and J. Male, *Journal of Physics and Chemistry of Solids*, 1964, **25**, 311–321.

[46] A. Di Bartolomeo, *Physics Reports*, 2016, **606**, 1–58.

[47] S. M. Sze and M. K. Lee, in *Semiconductor Devices: Physics and Technology*, Wiley, 3rd edn., 2012, pp. 2, 236–240.

[48] M. Liao, Y. Koide and J. Alvarez, *Applied Physics Letters*, 2006, **88**, 033504.

[49] C. Verona, in *Photodiodes-World Activities in 2011*, IntechOpen, 2011, ch. 13, pp. 315–332.

[50] S. Kasap, M. Kabir, K. O. Ramaswami, R. E. Johanson and R. J. Curry, *Journal of Applied Physics*, 2020, **128**, 124501.

[51] Y. Sato, H. Murakami, T. Shimaoka, M. Tsubota and J. H. Kaneko, *Nuclear Instruments and Methods in Physics Research Section A: Accelerators, Spectrometers, Detectors and Associated Equipment*, 2016, **834**, 218–222.

[52] G. Lioliou, G. Lefeuvre and A. Barnett, *Nuclear Instruments and Methods in Physics Research Section A: Accelerators, Spectrometers, Detectors and Associated Equipment*, 2021, **991**, 165025.

[53] C. Bodie, G. Lioliou, G. Lefeuvre and A. Barnett, *Applied Radiation and Isotopes*, 2022, **180**, 110027.

[54] S. Curtoni, M.-L. Gallin-Martel, S. Marcatili, L. Abbassi, A. Bes, G. Bosson, J. Collot, T. Crozes, D. Dauvergne, W. De Nolf, P. Everaere, L. Gallin-Martel, A. Ghimouz, F. Haddad, C. Hoarau, J.-Y. Hostachy, C. Koumeir, A. Lacoste, V. Métivier, J. Morse, J.-F. Motte, J.-F. Muraz, F. Poirier, F. Rarbi, O. Rossetto, M. Salomé, N. Servagent, E. Testa and M. Yamouni, *Nuclear Instruments and Methods in Physics Research Section A: Accelerators, Spectrometers, Detectors and Associated Equipment*, 2021, **1015**, 165757.

[55] E. Abubakr, S. Ohmagari, A. Zkria, H. Ikenoue and T. Yoshitake, *Materials Science in Semiconductor Processing*, 2022, **139**, 106370.

[56] C. N. Taylor, *Journal of Nuclear Materials*, 2022, **558**, 153396.

[57] Tritium; a radioactive isotope of hydrogen, https://www.radioactivity.eu.com/site/pages/Tritium.htm, (Accessed 19/11/21).

[58] K. Jang, D. Cho, W. Yoo, J. Seo, J. Heo, J.-Y. Park and B. Lee, *Nuclear Instruments and Methods in Physics Research Section A: Accelerators, Spectrometers, Detectors and Associated Equipment*, 2011, **652**, 928–931.

[59] P. Fichet, A. Bultel, S. Markelj and C. Moreno, *Review of the different techniques to analyse tritium*, TRANSAT, 2018.

[60] S. O'hira, Y. Edao, K. Isobe and Y. Iwai, *Fusion Engineering and Design*, 2021, **170**, 112502.

[61] J.-C. Arnault, S. Saada and V. Ralchenko, *physica status solidi (RRL), Rapid Research Letters*, 2021, 2100354.

[62] S. Linnik, S. Zenkin, A. Gaydaychuk and A. Mitulinsky, *Diamond and Related Materials*, 2021, **120**, 108681.

[63] J.-Y. Zhang, P.-F. Wang, S.-J. Ding, D. W. Zhang, J.-T. Wang and Z.-J. Liu, *Thin solid films*, 2000, **368**, 266–268.

[64] R. Haubner and B. Lux, *International Journal of Refractory Metals and Hard Materials*, 2002, **20**, 93–100.

[65] F. Hörmann, M. Schreck and B. Stritzker, *Diamond and related materials*, 2001, **10**, 1617–1621.

[66] J.-P. Lagrange, A. Deneuville and E. Gheeraert, *Diamond and Related Materials*, 1998, **7**, 1390–1393.

[67] J. Kim, F. Kim and J. Huang, *Materials today*, 2010, **13**, 28–38.

[68] A. Shivayogimath, P. R. Whelan, D. M. Mackenzie, B. Luo, D. Huang, D. Luo, M. Wang, L. Gammelgaard, H. Shi, R. S. Ruoff *et al.*, *Chemistry of Materials*, 2019, **31**, 2328–2336.

[69] M. Omidi, A. Fatehinya, M. Farahani, Z. Akbari, S. Shahmoradi, F. Yazdian, M. Tahriri, K. Moharamzadeh, L. Tayebi and D. Vashaee, *Biomaterials for oral and dental tissue engineering*, Elsevier, 2017, pp. 97–115.